Late Cretaceous Magmatism in the Sredinnyi Range of Kamchatka: Geochronology and Composition

A. V. Soloviev[a, b], M. V. Luchitskaya[b], O. B. Selyangin[c], and J. K. Hourigan[d]

[a]Open Joint-Stock Company Rosgeologiya, Khersonskaya ul. 43(3), Moscow, 117246 Russia
e-mail: fission-track@mail.ru
[b]Geological Institute (GIN RAN), Russian Academy of Sciences, Pyzhevskii per. 7, Moscow, 119017 Russia
[c]Scientific Research Geotechnological Center, Far East Branch, Russian Academy of Sciences,
Severo-Vostochnoe sh. 30, Petropavlovsk-Kamchatsky, 683002 Russia
[d]University of California, 1156 High St., Santa Cruz, CA 95064, USA
Received June 26, 2013; in final form April 17, 2014

Abstract—The new data obtained during thorough geological–structural, geochronological, petrographic, and petrochemical investigations of Late Cretaceous granitoids from the southern Sredinnyi Range in Kamchatka and zircon dating by the U−Pb SIMS and LA-ICPMS methods indicate that this region was characterized by intense granitoid magmatism in the Campanian (83.1 ± 2.0 to 76.2 ± 1.5 Ma). The Campanian granitoids mark initiation of the "newly formed" continental crust in Kamchatka. The composition of these Late Cretaceous rocks demonstrates similarity to high-alumina I-type granites. The data allow the Campanian stage of magmatic activity to be defined in southern Kamchatka.

Keywords: Campanian stage, granitoid magmatism, SIMS and LA-ICP-MS U−Pb dating, petrogeochemistry, Sredinnyi Range, Kamchatka

DOI: 10.1134/S0869593815010086

INTRODUCTION

Owing to the application of advanced geochronological methods for local rock dating, Late Cretaceous age of granitoid rocks in the southern Sredinnyi (Median) Range of Kamchatka is now reliably substantiated (Soloviev, 2008; Luchitskaya et al., 2008; Hourigan et al., 2009; Luchitskaya and Soloviev, 2010). Thus, the available extensive data are sufficient for defining the Campanian Stage in the granite formation in Kamchatka.

The Campanian gneissic granites documented in the southern Sredinnyi Range of Kamchatka as the Krutogorova Complex intrude metamorphic rocks of the Kolpakova Group (Khanchuk, 1985; Rikhter, 1995; Luchitskaya et al., 2008). Their age ranging from 83.1 ± 2.0 to 76.2 ± 1.5 Ma is substantiated U−Pb zircon dating (Table 1). These granitoids mark the initiation of the "newly formed" continental crust in Kamchatka. The purpose of this work is the detailed geological–structural, geochronological, petrographic, and petrogeochemical investigation of Late Cretaceous granitoids developed in the southern Sredinnyi Range for reconstructing the geodynamic settings of their formation on the basis of petrogeochemical and chronological properties of these rocks.

CRETACEOUS GRANITOIDS IN THE STRUCTURE OF THE SOUTHERN SREDINNYI RANGE

The Late Cretaceous granites (Luchitskaya et al., 2008; Hourigan et al., 2009) associate spatially with outcrops of metamorphic rocks in the Malka Uplift of Kamchatka (Fig. 1) (*Karta...*, 1999). The origin, age, and protolith nature of metamorphic rocks of the Sredinnyi Range of Kamchatka have been debated during the last 30 years (Lebedev, 1967; Marchenko, 1975; Khanchuk, 1985; Rikhter, 1995; *Gosudarstvennaya...*, 2006; Soloviev, 2006; Hourigan et al., 2009; Selyangin, 2009; etc.). Zhegalova (1978, 1981) was the first to establish the fold−thrust structure of metamorphic complexes of the Sredinnyi Range. This concept was further developed in subsequent works (Rikhter, 1995; Bondarenko, 1997; Kirmasov et al., 2004; Soloviev, 2008; Shapiro et al., 2008; Hourigan et al., 2009; Luchitskaya and Soloviev, 2012). According to the model substantiated by structural observations and geochronological data, the Kolpakova Group intruded by granitoids of the Krutogorova Complex is overlain by rocks of the Kamchatka Group (Shikhta Formation) and Kheivan Formation (Figs. 1, 2) (Shapiro et al., 2008; Luchitskaya and Soloviev, 2012). These units are attributed together with nonmetamorphosed rocks of the Khozgon Formation to the autochthon. The allochthon is represented by metamorphic rocks

Table 1. Composite geochronological data on Cretaceous igneous and orthometamorphic rocks from the southern Sredinnyi Range of Kamchatka

| Sample	Complex and rock type	Method, mineral	Latitude, N	Longitude, E	Age, Ma ($\pm 2\sigma$)	Source
02LG24	Krutogorova granite	U-Pb SIMS, zircon	54°50.564′	157°22.754′	78.5 ± 1.5	Hourigan et al., 2009
M-024/1	Krutogorova granite	U-Pb SIMS, zircon	54°29.907′	157°25.994′	80.2 ± 0.9	This work, Table 2
04AS99	Krutogorova granite	U-Pb SIMS, zircon	54°23.895′	157°09.081′	79.2 ± 1.9	This work, Table 3
04AS75	Orthogneiss	U-Pb SIMS, zircon	54°27.047′	157°11.512′	79.3 ± 0.9	This work, Table 4
M-438/1	Gneissic granite	U-Pb SIMS, zircon	54°27.405′	157°09.850′	83.1 ± 2.0	Luchitskaya and Soloviev, 2010
M-439/1	Gneissic granite	U-Pb SIMS, zircon	54°26.194′	157°09.650′	76.2 ± 1.5	Luchitskaya and Soloviev, 2010
M-427/1	Bimicaceous granite	U-Pb SIMS, zircon	54°32.472′	157°24.272′	81.1 ± 1.8	Luchitskaya and Soloviev, 2010
C10-3	Gneissic granite	U/Pb LA-ICPMS, zircon	Shanuch deposit		77.9 ± 1.4	This work, Table 5
C-11	Gneissic granite	U/Pb LA-ICPMS, zircon	Shanuch deposit		80.4 ± 1.2	This work, Table 5
	Krutogorova granite	U-Pb SIMS, zircon			80.0 ± 5.0	Gosudarstvennaya..., 2006
	Krutogorova granite	U-Pb SIMS, zircon			81.0 ± 2.5	Gosudarstvennaya..., 2006
	Kol'skii granite	U-Pb SIMS, zircon			80.0 ± 2.0	Gosudarstvennaya..., 2006

of the Andrianovka, Khimka, Irunei, and Kirganik formations. The metamorphic rocks of the Kolpakova Group intruded by gneissic granitoids of the Krutogorova Complex represent in fact a basement of the southern Sredinnyi Range.

The rocks of the *Kolpakova Group* intruded by Krutogorova gneissic granites form the lower structural stage of the autochthon. The Kolpakova Group is represented by migmatized sillimanite, kyanite, cordierite, cordierite−hypersthene, garnet−biotite, and biotite gneisses and plagiogneisses with rare intercalations of biotite−amphibole gneisses, garnet−clinopyroxene crystalline schists, amphibolites, garnet amphibolites, and metacarbonate rocks (Marchenko, 1976; Khanchuk, 1985; Tararin, 2008). The Kolpakova Group was primarily composed largely of sedimentary−terrigenous rocks of the diorite−tonalite composition with the dominant share of ferruginous varieties (Khanchuk, 1985) or volcanogenic−graywacke−clayey facies (Tararin, 1988; Rikhter, 1995). The protolith of amphibolites was likely represented by high-Ti oceanic basalts (Rikhter, 1995). The lenslike form of amphibolites bodies and the presence of metacarbonate rocks in mostly metaterrigenous

Fig. 1. Schematic geological structure of the southern Sredinnyi Range in Kamchatka (*Karta*..., 1999; Shapiro et al., 2008). (1) Quaternary sediments; (2) Miocene−Pliocene−Quaternary volcanics; (3) Eocene (?) volcanics of Mount Chernaya and Cherepanovka Formation; (4) Eocene−Oligocene marine and terrestrial sediments; (5−8) **allochthon**: (5) volcanogenic and sedimentary−volcanogenic sediments of the Kirganik Formation (Maastrichtian−Paleocene); (6−8) Santonian−Campanian siliceous−volcanogenic sediments and their nonmetamorphosed analogs of the Irunei (6), Khimka (7), and Andrianovka (8) formations; (9−12) **autochthon**: (9−11) Upper Cretaceous−Paleocene terrigenous sediments and their metamorphic analogs of the Khozgon (9), Kheivan and Stopol'nik (10) formations, and Kamchatka Group (Shikhta Formation) (11); (12) Lower and Upper Cretaceous metamorphic rocks of the Kolpakova Group; (13) Upper Jurassic−Early Cretaceous (?) volcanogenic rocks of the Kvakhona Group; (14) Late Cretaceous gneissic granites and granite−gneisses of the Krutogorova Complex; (15) Late Cretaceous (Campanian−Maastrichtian) pyroxene−gabbro−syenite intrusions; (16) early Eocene (?) ultramafic−mafic intrusions; (17) early Eocene granitoids; (18) thrusts: (a) main between the autochthon and allochthon, (b) secondary; (19) subvertical fractures: (a) main, (b) secondary; (20) assumed fractures: (a) main, (b) secondary.
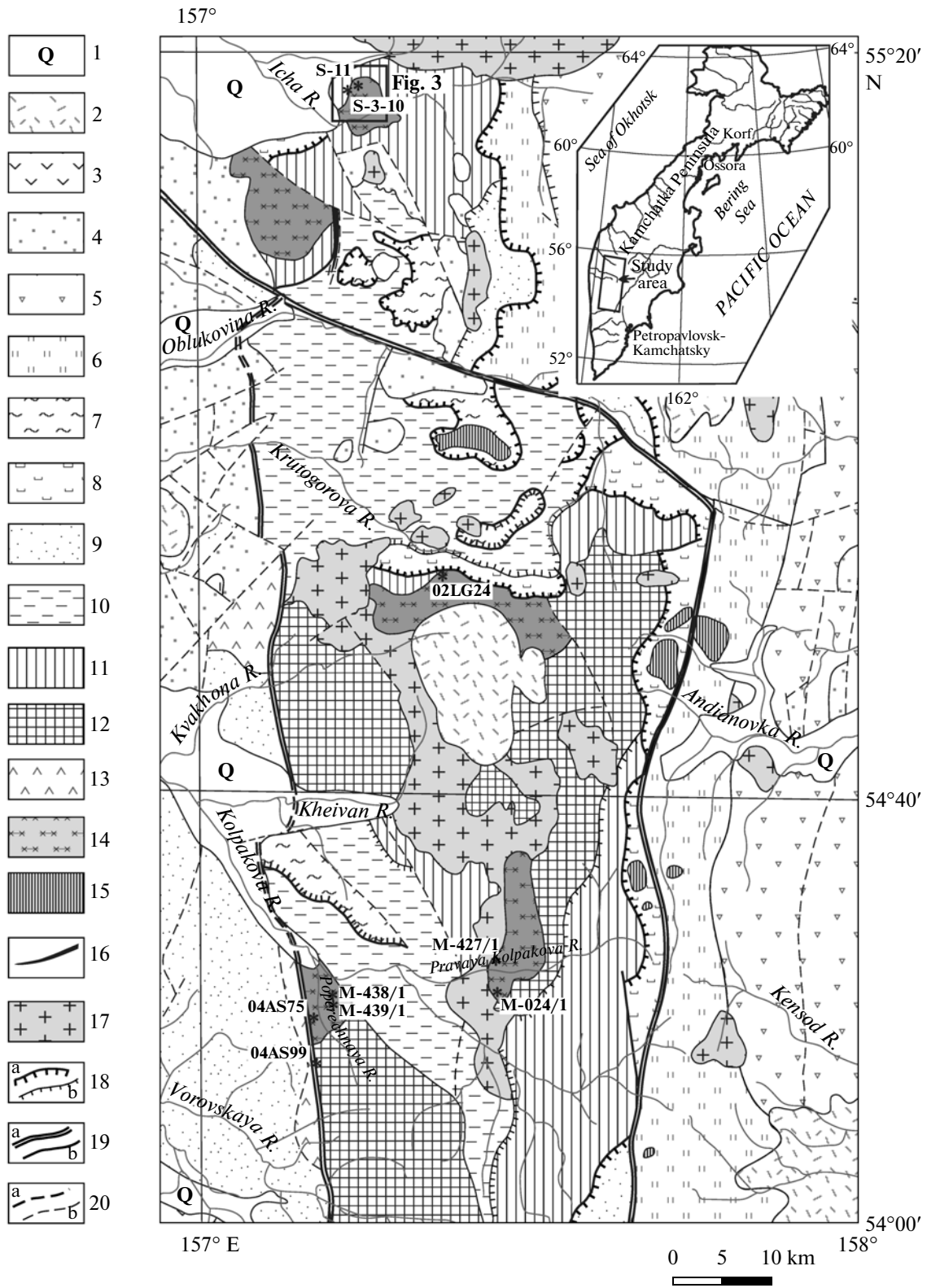
sequences allow the near-continental subduction–accretionary wedges to be considered as potential analogs of the Kolpakova Group (Khanchuk, 1985).

Granitoids of the Krutogorova Complex (Khanchuk, 1985; Rikhter, 1995; Soloviev, 2010), which intrude the Kolpakova Group, are dominated by gneissic varieties, although they include also equigranular rocks (Luchitskaya and Soloviev, 2010). According to the composition, the Krutogorova Complex is represented by biotite bimicaceous granites with garnet and their varieties barren of the latter. Our investigations revealed that granites of the Krutogorova Complex are characterized by a wider distribution than was previously thought.

The data on age of the Kolpakova Group are ambiguous, which is discussed in (Soloviev, 2008; Tararin, 2008). On the latest geological map, the protolith of the Kolpakova Group is shown as being the Proterozoic in age and two stages of its metamorphism are dated back to 140–127 and 70–60 Ma (*Gosudarstvennaya...*, 2006). The SIMS U–Pb dating of zircons from rocks of the Kolpakova Group indicates that the formation of the protolith of gneisses was in progress up to the terminal Early–initial Late Cretaceous (Soloviev, 2008; Hourigan et al., 2009). The age of gneissic granitoids of the Krutogorova Complex, which intrude the Kolpakova Group, is determined as ranging from 83.1 ± 2.0 to 76.2 ± 1.5 Ma (Fig. 1, Table 1). This age marks the upper limit of the Kolpakova Group formation. It should be noted that zircons from orthogneisses sampled on the right bank of the Poperechnaya River yielded a concordant age of 79.3 ± 0.9 Ma (Table 1, Fig, 1). The rims of zircons from rocks of the Kolpakova Group are dated back to 77 Ma (Bindeman et al., 2002). Similar dates of Krutogorova granitoids and metamorphic rocks of the Kolpakova Group imply the unity of the granite formation and metamorphism.

The rocks of the *Kamchatka Group* rest upon the Krutogorova granites, which intrude the Kolpakova Group, with unconformity and basal conglomerates at the base (Khanchuk, 1985; Rikhter, 1995). The group is largely represented by biotite schists and plagiogneisses with garnet, staurolite, kyanite, and sillimanite. The zircon dates obtained by the SIMS U–Pb method for rocks of the Kamchatka Group suggest that the protolith of its schists was accumulated in the Paleocene (Soloviev, 2008; Hourigan et al., 2009). The *Kheivan Formation* is composed of phyllites, metasandstones, and metasiltstones with subordinate mudstones and gravelites. The rocks are variably metamorphosed: from chlorite facies to biotite–garnet schists (Rikhter, 1995). The SIMS U–Pb dates of zircons from schists of the Kheivan Formation indicate the Early Cretaceous age of the protolith (Soloviev, 2008; Hourigan et al., 2009).

The allochthon of the Malka Uplift in the Sredinnyi Range of Kamchatka includes the Andrianovka and Khimka (Alistor) formations (Rikhter, 1995; Bondarenko, 1997; Shapiro et al., 2008). It is convincingly shown that the *Andrianovka Formation* is thrust onto either the Krutogorova granites or schists of the Kamchatka Group (Shikhta Formation); the base of the thrust is locally marked by serpentinite melange (Rikhter, 1995; Kirmasov et al., 2004). The Andrianovka Formation is composed of quartz–albite–actinolite–chlorite, quartz–feldspar–amphibole, epidote–amphibole, amphibole, and clinopyroxene–amphibole schists, quartzites, and amphibolites. The protolith of the Andrianovka Formation was likely formed in the early Late Cretaceous (Soloviev, 2008; Kuz'min et al., 2009). The *Khimka Formation* is represented by albite–actinolite schists of the chlorite subfacies developed after tuffs, tuffites, and metasandstones as well as by quartzites. It is believed that the *Alistor Formation* composed of amphibole schists is the facies and age analog of this unit (Khanchuk, 1985; Bondarenko, 1997). Geochronological data on the age of the Khimka Formation are absent.
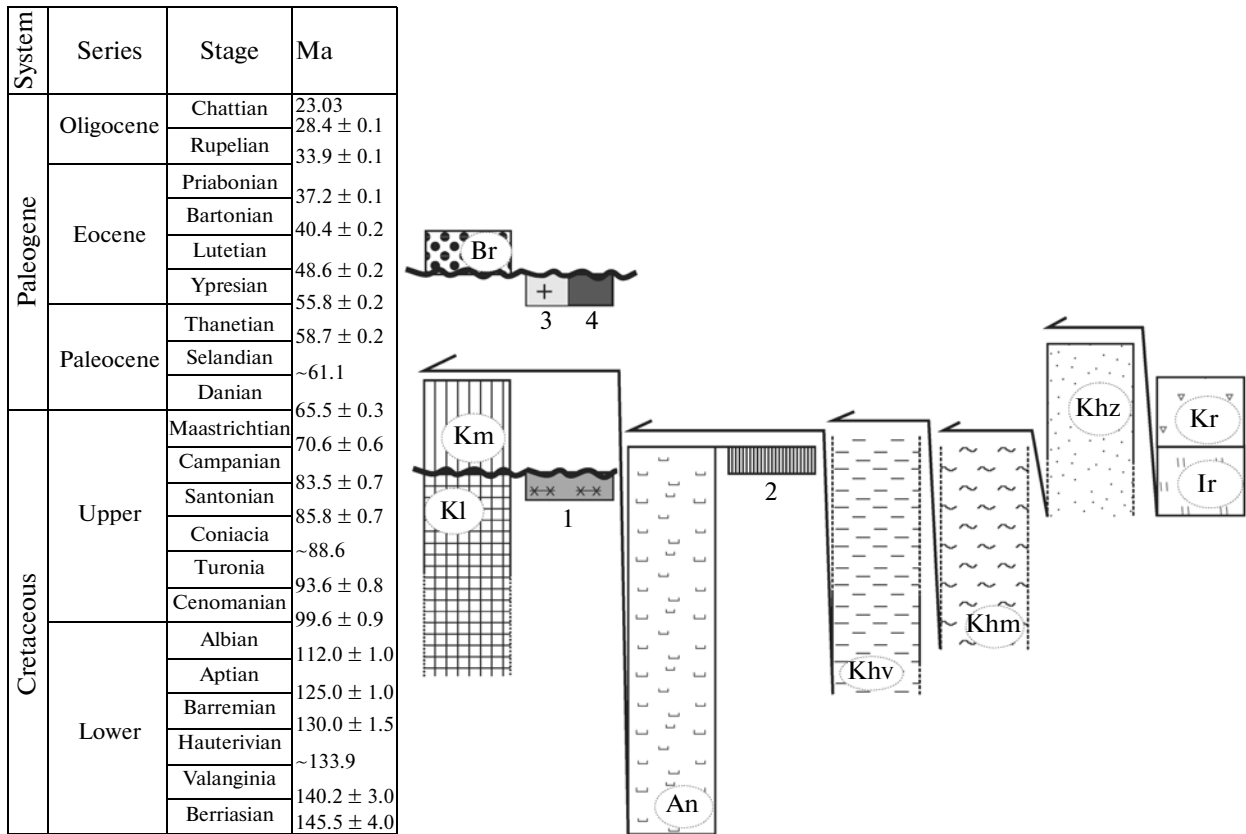
The early Eocene syncollisional metamorphism occurred at 52 ± 2 Ma (Soloviev, 2008; Hourigan et al., 2009). In the early Eocene, the rocks developed in the southern Stredinnyi Range of Kamchatka were subjected to migmatization and emplacement of granotoid bodies and norite–kortlandite intrusions (Fig. 2) (Konnikov et al., 2006; Luchitskaya and Soloviev, 2012).

The Baraba Formation composed of terrestrial conglomerates and unconformably resting upon metamorphic complexes represents a neoautochthon in the Sredinnyi Range fold–thrust structure (Figs. 1, 2). Zircons extracted from tuff of the basal layer of the Baraba Formation dated by the SIMS U–Pb method yielded an age of 50.5 ± 1.2 Ma (Soloviev et al., 2004), i.e., the terminal early Eocene. It should be noted that zircon from granitoid pebble sampled from the Baraba conglomerates is dated by the fission-track method (Soloviev et al., 2007). Its age of 83.3 ± 4.3 (±1σ) corresponds to the interval of formation of the Krutogorova granitoids. Thus, it may be stated that Late Cretaceous granitoids were exhumed to the erosion environments in the early Eocene.

CRETACEOUS GRANITOIDS OF THE SOUTHERN SREDINNYI RANGE OF KAMCHATKA

On the geological map of the third generation (*Gosudarstvennaya...*, 2006), the Krutogorova plutonic gneiss–plagiogranite complex is erroneously attributed to the Early Cretaceous, although Campanian ages obtained for the Krutogorova granitoids are mentioned even in its explanatory notes. At present, there are many data available (Tables 1–5) which allow the conclusion that the Krutogorova plutonic gneiss–plagiogranite and Kol'skii plagiogranite–granodiorite complexes were formed synchronously in the Late Cretaceous. It should be noted that all the U–Pb dates obtained for zircons from granitoids of both the Krutogorova and Kol'skii complexes fall into a very nar-

(a)

System	Series	Stage	Ma
	Oligocene	Chattian	23.03
			28.4 ± 0.1
		Rupelian	33.9 ± 0.1
	Eocene	Priabonian	37.2 ± 0.1
Paleogene		Bartonian	40.4 ± 0.2
		Lutetian	48.6 ± 0.2
		Ypresian	55.8 ± 0.2
	Paleocene	Thanetian	58.7 ± 0.2
		Selandian	~61.1
		Danian	65.5 ± 0.3
	Upper	Maastrichtian	70.6 ± 0.6
		Campanian	83.5 ± 0.7
		Santonian	85.8 ± 0.7
		Coniacia	~88.6
		Turonia	93.6 ± 0.8
Cretaceous		Cenomanian	99.6 ± 0.9
		Albian	112.0 ± 1.0
		Aptian	125.0 ± 1.0
	Lower	Barremian	130.0 ± 1.5
		Hauterivian	~133.9
		Valanginia	140.2 ± 3.0
		Berriasian	145.5 ± 4.0

(b)

Fig. 2. (a) Schematic stratigraphic and structural relations between lithological complexes in the southern Sredinnyi Range of Kamchatka; (b) milonitized bimicaceous granite (Sample 04AS99, 79.2 ± 1.9 Ma).

Neoautochthon: (Br) terrigenous rocks of the Baraba Formation; **allochthon**: (Kr) volcanogenic and sedimentary–volcanogenic rocks of the Kirganik Formation; (Ir, Khm, An) siliceous–volcanogenic rocks and their metamorphosed analogs of the Irunei, Khimka, and Andrianovka formations, respectively; **autochthon**: (Khz, Khv, Km) terrigenous rocks and their metamorphic analogs of the Khozgon, Kheivan formations, and Kamchatka Group (Shikhta Formation), respectively; (Kl) metamorphic rocks of the Kolpakova Group; **igneous rocks**: (1) gneissic granites and granite–gneisses of the Krutogorova Complex (83.1 ± 2.0 to 76.2 ± 1.5 Ma; Table 1), (2) pyroxene–gabbro–syenite intrusions (70.4 ± 0.7 to 63.0 ± 0.6 Ma; Hourigan et al., 2004), (3) intrusions of the norite–kortlandite formation (55–49 Ma; Konnikov et al., 2006; Luchitskaya and Soloviev, 2012), (4) granitoids (54.9 ± 0.5 to 50.1 ± 1.7 Ma; Luchitskaya and Soloviev, 2012). Arrows indicate thrusts.

Table 2. U−Pb SIMS isotopic data on zircons from gneissic granites (Sample M-024/1) of the Krutogorova Complex, Pravaya Kolpakova River (54°29.907′ N, 157°25.994′ E, altitude 880 m)

Point number	$^{206}Pb_{@обыкн}$, %	U, ppm	Th, ppm	Th/U	Noncorrected		^{207}Pb-corrected	
					$^{238}U/^{206}Pb$	$^{207}Pb/^{206}Pb$	$^{206}Pb/^{238}U$ age, Ma	
M024/1-1	0.47	76	36	0.49	86.26 ± 2.8	0.0512 ± 0.0049	74.0 ± 2.1	†
M024/1-2	0.17	1245	51	0.04	81.52 ± 1.1	0.0489 ± 0.0012	78.5 ± 0.9	
M024/1-3	0.39	225	109	0.50	79.60 ± 1.7	0.0507 ± 0.0028	80.2 ± 1.4	
M024/1-4	0.46	314	247	0.81	79.11 ± 1.5	0.0513 ± 0.0023	80.6 ± 1.2	
M024/1-5	—	607	35	0.06	78.62 ± 1.4	0.0471 ± 0.0016	81.5 ± 1.1	
M024/1-6	0.71	514	29	0.06	79.28 ± 1.3	0.0533 ± 0.0019	80.2 ± 1.1	
M024/1-7	—	377	105	0.29	78.73 ± 1.4	0.0464 ± 0.0020	81.5 ± 1.2	
M024/1-8	0.18	232	80	0.36	79.54 ± 1.7	0.0490 ± 0.0026	80.4 ± 1.4	
M024/1-9	—	238	46	0.20	82.04 ± 1.7	0.0452 ± 0.0026	78.3 ± 1.3	
M024/1-10	—	354	51	0.15	77.90 ± 1.5	0.0444 ± 0.0020	82.6 ± 1.2	
M024/1-11	0.57	324	31	0.10	79.12 ± 1.5	0.0522 ± 0.0022	80.5 ± 1.2	
M024/1-12	0.05	245	33	0.14	79.92 ± 1.7	0.0480 ± 0.0025	80.1 ± 1.3	
M024/1-13	—	99	33	0.35	82.75 ± 2.4	0.0448 ± 0.0039	77.7 ± 1.9	
						Average weighted $^{206}Pb/^{238}U$ age of 80.2 ± 0.9 Ma (95% confidence interval) $n = 12/13$ MSWD = 1.27, probability 0.23%		

(†) Omitted discordant ages.

Table 3. U−Pb SIMS isotopic data on zircons from milonitized granites (Sample 04AS99) of the Krutogorova Complex, Poperechnaya River (54°23.895′ N, 157°09.081′ E, altitude 1130 m)

Point number	$^{206}Pb_{@обыкн}$, %	U, ppm	Th, ppm	Th/U	Noncorrected		^{207}Pb-corrected	
					$^{238}U/^{206}Pb$	$^{207}Pb/^{206}Pb$	$^{206}Pb/^{238}U$ age, Ma	
AS99-1	0.74	269	64	0.25	87.25 ± 1.7	0.0534 ± 0.0027	72.9 ± 1.2	†
AS99-2	—	369	92	0.26	78.49 ± 1.4	0.0466 ± 0.0020	81.7 ± 1.2	
AS99-3	0.13	1787	80	0.05	83.97 ± 1.1	0.0486 ± 0.0010	76.2 ± 0.8	†
AS99-4	0.32	310	69	0.23	75.74 ± 1.5	0.0503 ± 0.0023	84.3 ± 1.3	†
AS99-5	0.38	439	101	0.24	81.24 ± 1.4	0.0506 ± 0.0019	78.6 ± 1.1	
AS99-6	0.01	2508	222	0.09	68.82 ± 1.0	0.0480 ± 0.0007	93.0 ± 0.9	†
AS99-7	0.28	1769	436	0.25	75.13 ± 1.0	0.0499 ± 0.0009	85.0 ± 0.9	†
AS99-8	—	1116	277	0.26	77.57 ± 1.1	0.0463 ± 0.0011	82.7 ± 0.9	†
AS99-9	—	657	93	0.15	74.41 ± 1.2	0.0472 ± 0.0014	86.1 ± 1.1	†
AS99-10	0.07	201	47	0.24	79.45 ± 1.8	0.0482 ± 0.0027	80.6 ± 1.4	
AS99-11	—	703	142	0.21	81.14 ± 1.2	0.0460 ± 0.0014	79.1 ± 1.0	
AS99-12	0.06	438	135	0.32	81.02 ± 1.4	0.0480 ± 0.0018	79.0 ± 1.1	
AS99-13	—	303	45	0.15	81.04 ± 1.5	0.0439 ± 0.0021	79.4 ± 1.2	
AS99-14	0.98	211	71	0.35	80.68 ± 1.7	0.0553 ± 0.0029	78.6 ± 1.4	
AS99-15	0.23	432	4	0.01	82.80 ± 1.4	0.0494 ± 0.0019	77.2 ± 1.1	
						Average weighted $^{206}Pb/^{238}U$ age of 79.2 ± 1.9 Ma (95% confidence interval) $n = 8/15$ MSWD = 1.34, probability 0.23%		

(†) Omitted discordant ages and grains with high U concentrations.

Table 4. U−Pb SIMS isotopic data on zircons from orthogneiss (Sample 04AS75) of the Krutogorova Complex, Poperechnaya River (54°27.047′ N, 157°11.512′ E, altitude 1034 m)

Point number	$^{206}Pb_{@обыкн}$, %	U, ppm	Th, ppm	Th/U	Noncorrected		^{207}Pb-corrected	
					$^{238}U/^{206}Pb$	$^{207}Pb/^{206}Pb$	$^{206}Pb/^{238}U$ age, Ma	
AS75-1	0.84	232	69	0.31	78.44 ± 1.7	0.0543 ± 0.0027	81.0 ± 1.4	
AS75-2	0.44	421	243	0.60	82.14 ± 1.4	0.0510 ± 0.0020	77.7 ± 1.1	
AS75-3	0.06	317	184	0.60	79.41 ± 1.5	0.0481 ± 0.0021	80.6 ± 1.2	
AS75-4	0.28	678	500	0.76	79.56 ± 1.2	0.0498 ± 0.0014	80.3 ± 1.0	
AS75-5	0.38	242	26	0.11	82.12 ± 1.6	0.0505 ± 0.0025	77.7 ± 1.3	
AS75-6	–	191	57	0.31	76.01 ± 1.8	0.0450 ± 0.0026	84.5 ± 1.5	†
AS75-7	–	208	103	0.51	80.11 ± 1.7	0.0453 ± 0.0026	80.2 ± 1.4	
AS75-8	0.31	273	62	0.24	81.76 ± 1.6	0.0500 ± 0.0024	78.1 ± 1.2	
AS75-9	–	555	367	0.68	55.12 ± 1.2	0.0466 ± 0.0013	116.2 ± 1.4	†
AS75-10	–	1345	49	0.04	74.91 ± 1.1	0.0470 ± 0.0010	85.6 ± 0.9	†
AS75-11	0.00	142	26	0.19	84.07 ± 2.0	0.0475 ± 0.0031	76.2 ± 1.6	
AS75-12	0.77	238	106	0.46	80.12 ± 1.6	0.0537 ± 0.0026	79.4 ± 1.3	
AS75-13	–	463	281	0.63	79.52 ± 1.3	0.0473 ± 0.0017	80.6 ± 1.1	

Average weighted $^{206}Pb/^{238}U$ age

79.3 ± 0.9 Ma (95% confidence interval)

$n = 10/13$

MSWD = 1.55, probability 0.12%

(†) Omitted discordant ages and grains with high U concentrations.

row age range marked by granitoid magmatism in the Campanian (Table 1).

The Cretaceous granitoids are developed in the southern (Pravaya Kolpakova and Poperechnaya river basins), central (upper reaches of the Krutogorova River), and northern (Oblukovina and Icha river basins) parts of the Malka Uplift in the Sredinnyi Range of Kamchatka (Fig. 1). The largest massifs, Levoozernovskii, Krutogorova, and Pravyi Kol, are confined to the Shanuch, Khangar, and Pymta granite−gneiss domes, respectively (*Gosudarstvennaya...*, 2006). The massifs are largely composed of gneissic plagiogranites, granodiorites, tonalities, granites, and, locally, diorites.

The Krutogorova massif located in the central part of the Khangar dome represents a petrological type of the synonymous complex (Khanchuk, 1985; *Gosudarstvennaya...*, 2006). The massif is represented by gneissic plagiogranites, granodiorites, tonalities, granites, and diorites. Granitoids of the massif intrude gneisses and migmatites of the Kolpakova Group. The boundaries of the massif are locally distinct, although they are usually vague, being characterized by complex relationships with gneisses. Migmatization and partial melting transformed the contact zone and apical part

of intrusion into a mixture of gneiss−granites and migmatites. The contact zone is locally marked by apophyses of granitoids in host rocks and their abundant xenoliths. The contact plane is usually parallel to banded patterns in intrusions and gneisses (*Gosudarstvennaya...*, 2006).

The Krutogorova massif and host rocks of the Kolpakova Group are overlain by rocks of the Kamchatka Group (Shikhta Formtion) (Khanchuk, 1985; Rikhter, 1995). The stratigraphic contact between these units is unconformable with conglomerates at the base of the last formation. The gneissic patterns in granitoids are reflected in the oriented arrangement of mica flakes, plagioclase, and, less commonly, hornblende. Orientation of gneissic bands in granitoids and host gneisses of the Kolpakova Group coincides with each other, which indicates, in the opinion of Khanchuk (1985), subsynchronous metamorphism of the Kolpakova Group and formation of the Krutogorova granites. The orientation of secondary shistosity in granites and rocks of the Malka Groups coincides with each other, reflecting the later stage of tectonic movements and metamorphism in common for all these rocks (Rikhter, 1995). Zircons from gneissic granites (Sample 021G24, Fig. 1, Table 1) taken from the Kru-

Table 5. U–Pb LA-ICPMS isotopic data on zircons from gneissic granites (Sredinnyi Range, Shanuch deposit area)

Point number	U, ppm	Th, ppm	U/Th	Isotope ratio							Apparent ages, M						Age, Ma	
				207Pb*/206Pb*	±	207Pb*/235U*	±	206Pb*/238U	±	error corr.	206Pb*/238U*	±	207Pb*/235U	±	207Pb*/206Pb*	±	Age	±2σ
Sample C10-3																		
C10_3_1	1396.0	66.9	21.2	0.1127	0.0037	0.1564	0.0075	0.0101	0.0005	0.36	64.6	2.9	147.2	6.6	1843.4	46.6	x	x
C10_3_3	267.5	36.9	7.4	0.1376	0.0094	0.1970	0.0160	0.0105	0.0005	0.20	67.1	3.2	180.0	13.0	2197.2	113.6	x	x
C10_3_1	1736.0	156.3	11.2	0.0877	0.0024	0.1274	0.0055	0.0107	0.0005	0.46	68.7	3.3	121.8	5.0	1375.9	35.1	x	x
C10_3_5	385.2	138.3	2.9	0.0504	0.0024	0.0769	0.0044	0.0111	0.0005	0.04	71.4	3.2	75.3	4.1	213.5	101.1	71.2	3.2
C10_3_6	936.0	107.6	8.9	0.0535	0.0018	0.0832	0.0040	0.0112	0.0005	0.11	71.8	3.2	81.0	3.7	350.1	59.2	x	x
C10_3_1	604.0	108.2	5.7	0.0553	0.0020	0.0876	0.0044	0.0114	0.0005	0.36	73.0	3.2	85.1	4.1	424.4	68.6	x	x
C10_3_2	862.0	92.2	9.3	0.0505	0.0015	0.0806	0.0038	0.0113	0.0005	0.27	72.7	3.2	78.8	3.6	218.1	55.0	72.4	3.2
C10_3_4	739.0	398.0	2.1	0.0493	0.0016	0.0779	0.0037	0.0114	0.0005	0.37	72.8	3.2	76.2	3.6	162.1	56.9	72.6	3.2
C10_3_1	595.1	163.0	3.8	0.0496	0.0027	0.0770	0.0047	0.0114	0.0005	0.03	73.2	3.3	75.4	4.5	176.3	117.6	72.9	3.3
C10_3_4	326.0	48.5	6.8	0.0729	0.0028	0.1197	0.0061	0.0119	0.0005	0.00	76.0	3.4	114.7	5.6	1011.2	66.7	x	x
C10_3_2	884.0	65.6	14.0	0.0756	0.0034	0.1276	0.0076	0.0119	0.0005	0.45	76.4	3.4	121.2	6.8	1084.5	79.6	x	x
C10_3_4	296.1	90.6	3.3	0.0506	0.0018	0.0801	0.0040	0.0116	0.0005	0.29	74.2	3.3	78.1	3.8	222.6	68.6	73.9	3.2
C10_3_2	325.2	92.9	3.5	0.0581	0.0027	0.0945	0.0055	0.0118	0.0005	0.27	75.5	3.4	91.0	5.0	533.5	90.4	x	x
C10_3_4	307.1	96.6	3.2	0.0544	0.0022	0.0891	0.0047	0.0118	0.0005	0.13	75.5	3.4	87.1	4.4	387.6	78.4	x	x
C10_3_8	457.0	43.9	9.9	0.0482	0.0030	0.0778	0.0054	0.0117	0.0005	0.11	74.9	3.4	76.6	5.1	109.1	137.2	74.9	3.5
C10_3_3	421.3	120.0	3.8	0.0479	0.0015	0.0769	0.0036	0.0117	0.0005	0.22	75.1	3.3	75.2	3.4	94.3	59.3	75.0	3.3
C10_3_1	851.0	200.0	4.4	0.0535	0.0024	0.0889	0.0050	0.0118	0.0005	0.05	75.9	3.4	86.4	4.6	350.1	93.0	x	x
C10_3_1	926.0	246.0	4.2	0.0467	0.0025	0.0758	0.0046	0.0118	0.0005	−0.01	75.3	3.4	73.9	4.3	33.9	118.0	75.4	3.5
C10_3_3	1004.0	113.7	9.1	0.1046	0.0071	0.1900	0.0160	0.0127	0.0006	0.73	81.2	3.6	174.0	13.0	1707.3	119.6	x	x
C10_3_2	224.7	44.7	5.0	0.0583	0.0034	0.0976	0.0064	0.0119	0.0006	0.05	76.5	3.5	94.7	6.0	541.1	120.0	x	x
C10_3_3	1885.0	224.0	8.9	0.0485	0.0016	0.0791	0.0038	0.0118	0.0005	0.36	75.8	3.3	77.4	3.6	123.7	63.1	75.7	3.3
C10_3_2	536.4	120.7	4.5	0.0476	0.0017	0.0805	0.0039	0.0118	0.0005	0.17	75.9	3.4	78.5	3.7	79.4	74.8	75.9	3.4
C10_3_2	229.7	66.9	3.7	0.0551	0.0014	0.0916	0.0039	0.0120	0.0005	0.42	76.7	3.4	89.0	3.6	417.9	36.1	x	x
C10_3_4	478.0	107.4	4.5	0.0576	0.0049	0.0939	0.0084	0.0122	0.0006	0.00	77.8	3.6	90.4	7.8	514.6	183.1	x	x
C10_3_5	782.0	146.8	5.5	0.0553	0.0021	0.0937	0.0048	0.0121	0.0005	0.13	77.7	3.5	90.9	4.4	424.4	68.6	x	x
C10_3_3	210.3	45.4	5.0	0.0511	0.0043	0.0867	0.0079	0.0121	0.0006	0.10	77.3	3.7	83.8	7.3	245.3	189.3	77.0	3.6
C10_3_2	100.9	30.1	3.3	0.0476	0.0011	0.0803	0.0034	0.0121	0.0005	0.38	77.3	3.4	78.4	3.2	78.4	31.4	77.3	3.4
C10_3_1	129.3	35.1	3.8	0.0475	0.0018	0.0804	0.0042	0.0121	0.0005	0.25	77.4	3.4	78.3	3.9	74.4	75.1	77.3	3.4
C10_3_2	1750.0	186.4	9.3	0.0481	0.0012	0.0805	0.0034	0.0121	0.0005	0.41	77.6	3.4	78.6	3.2	102.2	33.9	77.5	3.4
C10_3_9	475.0	55.9	8.2	0.0495	0.0015	0.0844	0.0039	0.0122	0.0005	0.25	78.1	3.4	82.1	3.6	171.6	51.9	77.9	3.4
C10_3_3	2166.0	176.0	12.6	0.0493	0.0012	0.0831	0.0035	0.0122	0.0005	0.32	78.2	3.4	81.1	3.3	162.6	34.6	78.0	3.4
C10_3_7	2092.0	115.6	18.2	0.0474	0.0016	0.0802	0.0038	0.0122	0.0005	0.26	78.1	3.5	78.3	3.6	69.4	65.2	78.1	3.4
C10_3_4	317.8	86.0	3.8	0.0470	0.0014	0.0796	0.0036	0.0122	0.0005	0.27	78.3	3.4	77.7	3.4	49.2	55.9	78.4	3.4
C10_3_1	444.0	104.4	4.5	0.0526	0.0021	0.0911	0.0048	0.0124	0.0006	0.20	79.2	3.5	88.3	4.4	311.6	77.9	x	x

Table 5. (Contd.)

Point number	U, ppm	Th, ppm	U/Th	Isotope ratio							Apparent ages, M						Age, Ma	
				$^{207}Pb^*/^{206}Pb^*$	±	$^{207}Pb^*/^{235}U^*$	±	$^{206}Pb^*/^{238}U$	±	error corr.	$^{206}Pb^*/^{238}U^*$	±	$^{207}Pb^*/^{235}U$	±	$^{207}Pb^*/^{206}Pb^*$	±		±2σ
C10_3_4	1284.0	85.2	16.0	0.0490	0.0022	0.0855	0.0048	0.0124	0.0006	0.16	79.6	3.7	83.1	4.5	147.8	95.7	79.5	3.7
C10_3_3	862.0	90.4	9.7	0.0737	0.0042	0.1358	0.0091	0.0129	0.0006	0.28	82.9	3.9	128.1	8.1	1033.3	109.7	x	x
C10_3_4	418.0	73.3	5.8	0.0478	0.0019	0.0824	0.0043	0.0125	0.0006	0.19	80.2	3.6	80.2	4.0	89.4	79.3	80.2	3.6
C10_3_4	540.0	224.0	2.4	0.0569	0.0025	0.1007	0.0058	0.0127	0.0006	0.31	81.4	3.7	97.4	5.4	487.7	85.3	x	x
C10_3_1	1095.0	68.0	14.7	0.0511	0.0024	0.0897	0.0052	0.0127	0.0006	0.15	81.1	3.7	86.9	4.9	245.3	99.2	80.7	3.7
C10_3_4	452.0	221.0	2.5	0.0475	0.0019	0.0826	0.0043	0.0126	0.0006	0.12	80.8	3.6	80.6	4.0	74.4	85.1	80.8	3.6
C10_3_2	267.2	64.9	4.4	0.0500	0.0013	0.0883	0.0039	0.0127	0.0006	0.28	81.2	3.5	85.9	3.6	192.7	40.5	80.9	3.5
C10_3_1	1572.0	81.5	19.9	0.0481	0.0013	0.0850	0.0037	0.0127	0.0006	0.32	81.3	3.6	82.9	3.5	101.7	41.3	81.3	3.6
C10_3_4	1628.0	87.7	18.9	0.0536	0.0018	0.0969	0.0048	0.0128	0.0006	0.25	82.0	3.6	93.7	4.5	354.3	63.2	x	x
C10_3_3	265.0	118.0	2.6	0.0469	0.0024	0.0828	0.0051	0.0127	0.0006	0.18	81.3	3.7	80.7	4.8	44.1	112.1	81.4	3.8
C10_3_2	655.0	87.4	8.2	0.0463	0.0016	0.0807	0.0040	0.0127	0.0006	0.25	81.5	3.6	78.9	3.7	13.3	67.5	81.6	3.6
C10_3_3	372.6	49.6	7.6	0.0503	0.0020	0.0905	0.0048	0.0130	0.0006	0.11	83.5	3.7	87.7	4.4	208.9	78.4	83.2	3.7
C10_3_3	229.7	64.9	3.7	0.0478	0.0012	0.0863	0.0037	0.0130	0.0006	0.45	83.5	3.7	84.1	3.5	90.4	35.2	83.4	3.7
C10_3_1	330.0	50.2	6.7	0.0465	0.0022	0.0846	0.0051	0.0131	0.0006	0.27	83.9	3.8	82.4	4.7	23.6	103.2	84.0	3.8
C10_3_3	308.0	58.3	6.5	0.0483	0.0020	0.0877	0.0048	0.0132	0.0006	0.25	84.4	3.8	85.1	4.4	114.0	83.0	84.4	3.8
C10_3_2	343.0	79.8	4.2	0.0470	0.0021	0.0858	0.0050	0.0132	0.0006	0.27	84.7	3.9	83.9	4.5	49.2	96.5	84.6	3.9

Average weighted $^{206}Pb/^{238}U$ age of 77.9 ± 1.4 Ma (±2σ), n = 31/50, MSWD = 4.7, probability 1.8%

Sample C-11

Point number	U, ppm	Th, ppm	U/Th	$^{207}Pb^*/^{206}Pb^*$	±	$^{207}Pb^*/^{235}U^*$	±	$^{206}Pb^*/^{238}U$	±	error corr.	$^{206}Pb^*/^{238}U^*$	±	$^{207}Pb^*/^{235}U$	±	$^{207}Pb^*/^{206}Pb^*$	±	Age	±2σ
C11_11	246.7	43.5	6.0	0.0472	0.0028	0.0730	0.0050	0.0112	0.0005	0.17	71.8	3.2	72.0	4.8	59.4	131.3	71.9	3.3
C11_42	226.7	59.2	4.0	0.0507	0.0028	0.0786	0.0050	0.0115	0.0005	0.06	73.5	3.3	76.5	4.7	227.2	118.5	73.2	3.3
C11_6	231.0	61.6	3.7	0.0485	0.0015	0.0764	0.0036	0.0116	0.0005	0.24	74.0	3.2	74.8	3.4	123.7	53.4	73.9	3.3
C11_7	806.0	50.6	15.3	0.0472	0.0025	0.0780	0.0050	0.0117	0.0005	0.23	74.8	3.4	76.5	4.8	59.4	116.1	74.9	3.4
C11_47	189.0	53.8	3.3	0.0555	0.0036	0.0891	0.0063	0.0119	0.0005	0.00	76.3	3.5	87.1	5.8	432.4	136.5	x	x
C11_48	241.0	73.0	3.9	0.0462	0.0032	0.0765	0.0059	0.0118	0.0006	0.10	75.7	3.5	74.3	5.5	8.1	161.5	75.9	3.5
C11_34	273.2	89.2	3.2	0.0601	0.0029	0.0994	0.0057	0.0121	0.0005	0.12	77.3	3.5	96.2	5.3	607.2	93.6	x	x
C11_17	303.0	101.6	2.8	0.0484	0.0023	0.0802	0.0046	0.0120	0.0005	0.07	76.7	3.5	78.9	4.3	118.9	102.3	76.6	3.4
C11_45	199.4	33.8	5.8	0.0483	0.0015	0.0801	0.0037	0.0120	0.0005	0.13	76.8	3.4	78.3	3.5	114.0	58.6	76.8	3.4
C11_50	126.2	20.2	6.3	0.0516	0.0029	0.0873	0.0057	0.0121	0.0006	0.04	77.3	3.5	84.6	5.3	267.7	120.0	76.9	3.6
C11_2	626.0	217.0	3.0	0.0480	0.0016	0.0789	0.0038	0.0120	0.0005	0.22	77.0	3.4	77.0	3.6	99.3	64.1	76.9	3.4
C11_22	670.8	112.7	6.1	0.0534	0.0029	0.0886	0.0057	0.0122	0.0006	0.03	78.4	3.5	86.2	5.3	345.8	114.4	x	x
C11_32	295.3	40.6	7.6	0.0486	0.0015	0.0817	0.0037	0.0122	0.0005	0.18	78.2	3.4	79.8	3.5	128.6	53.3	78.1	3.4
C11_37	432.0	89.7	4.7	0.2060	0.0190	0.4940	0.0560	0.0153	0.0008	0.81	97.7	5.1	379.0	38.0	2874.3	142.0	x	x
C11_49	2468.0	140.2	17.6	0.0486	0.0013	0.0816	0.0035	0.0123	0.0005	0.05	78.7	3.4	79.6	3.3	127.6	40.7	78.6	3.4
C11_43	316.0	59.6	5.1	0.0488	0.0021	0.0823	0.0046	0.0123	0.0006	0.13	78.7	3.5	80.4	4.2	138.2	91.4	78.6	3.5
C11_16	692.5	34.5	27.5	0.0440	0.0029	0.0739	0.0054	0.0123	0.0006	0.02	78.7	3.7	72.6	5.2	−110.7	151.1	79.0	3.7
C11_44	743.0	27.9	29.6	0.0488	0.0014	0.0828	0.0037	0.0124	0.0005	0.25	79.6	3.5	80.7	3.5	137.3	46.7	79.5	3.4

Table 5. (Contd.)

Point number	U, ppm	Th, ppm	U/Th	Isotope ratio $\frac{^{207}Pb^*}{^{206}Pb^*}$	±	$\frac{^{207}Pb^*}{^{235}U^*}$	±	$\frac{^{206}Pb^*}{^{238}U}$	±	error corr.	Apparent ages, M $\frac{^{206}Pb^*}{^{238}U^*}$	±	$\frac{^{207}Pb^*}{^{235}U}$	±	$\frac{^{207}Pb^*}{^{206}Pb^*}$	±	Age, Ma	±2σ
C11_25	245.1	58.1	4.3	0.0478	0.0011	0.0822	0.0035	0.0124	0.0006	0.48	79.5	3.5	80.2	3.3	91.4	29.7	79.5	3.5
C11_10	1234.0	81.1	15.1	0.0482	0.0013	0.0819	0.0036	0.0124	0.0005	0.17	79.6	3.5	79.9	3.4	107.1	44.1	79.6	3.4
C11_1	1086.0	75.3	14.2	0.0491	0.0013	0.0840	0.0036	0.0124	0.0005	0.18	79.8	3.5	82.0	3.4	153.1	40.1	79.6	3.4
C11_20	1057.0	60.0	17.7	0.0477	0.0019	0.0805	0.0043	0.0124	0.0006	0.07	79.7	3.5	78.5	4.0	84.4	79.6	79.7	3.5
C11_12	1321.0	62.4	21.8	0.0479	0.0013	0.0821	0.0036	0.0125	0.0006	0.33	80.3	3.5	80.1	3.4	91.9	40.6	80.2	3.5
C11_33	514.0	85.1	6.1	0.0491	0.0015	0.0856	0.0039	0.0126	0.0006	0.22	80.7	3.5	83.3	3.7	152.6	52.5	80.6	3.5
C11_41	1222.0	70.3	17.6	0.0476	0.0025	0.0810	0.0049	0.0126	0.0006	0.04	80.6	3.7	79.1	4.5	79.4	114.7	80.6	3.7
C11_35	313.0	117.1	2.7	0.0486	0.0013	0.0841	0.0037	0.0126	0.0006	0.27	80.8	3.5	82.0	3.5	130.5	43.5	80.7	3.6
C11_18	1226.0	101.3	11.8	0.0469	0.0015	0.0827	0.0039	0.0127	0.0006	0.20	81.2	3.6	80.8	3.6	44.1	61.2	81.2	3.6
C11_40	590.1	78.1	7.5	0.0483	0.0024	0.0862	0.0053	0.0127	0.0006	0.14	81.4	3.7	84.0	4.8	114.0	102.6	81.4	3.7
C11_15	719.0	75.1	10.0	0.0478	0.0014	0.0836	0.0038	0.0128	0.0006	0.15	82.3	3.6	81.5	3.5	89.4	49.6	82.2	3.6
C11_46	1387.0	76.6	18.3	0.0464	0.0016	0.0829	0.0041	0.0128	0.0006	0.35	82.2	3.7	80.8	3.8	18.5	67.3	82.4	3.7
C11_14	1196.0	57.8	21.1	0.0484	0.0013	0.0855	0.0037	0.0130	0.0006	0.31	82.9	3.6	83.3	3.5	118.4	41.4	82.9	3.6
C11_36	251.0	71.3	3.5	0.0474	0.0013	0.0850	0.0037	0.0130	0.0006	0.37	83.2	3.6	82.8	3.5	71.4	41.6	83.2	3.6
C11_4	917.0	74.5	12.5	0.0494	0.0031	0.0877	0.0064	0.0131	0.0006	0.16	83.6	3.9	85.1	5.9	166.9	137.2	83.4	3.9
C11_38	652.0	98.3	7.2	0.0476	0.0026	0.0850	0.0055	0.0130	0.0006	0.19	83.5	3.8	82.8	5.1	79.4	119.7	83.5	3.8
C11_5	1255.0	88.9	13.8	0.0466	0.0015	0.0842	0.0040	0.0130	0.0006	0.16	83.5	3.7	81.9	3.7	28.8	61.7	83.6	3.7
C11_9	155.9	34.2	4.6	0.0495	0.0013	0.0894	0.0039	0.0131	0.0006	0.20	83.8	3.7	86.9	3.6	170.6	40.6	83.6	3.7
C11_19	281.0	65.2	4.8	0.0413	0.0036	0.0738	0.0070	0.0130	0.0006	0.17	82.9	3.9	71.8	6.6	269.0	215.3	x	x
C11_27	136.4	47.3	3.2	0.0489	0.0022	0.0881	0.0050	0.0131	0.0006	0.20	84.0	3.8	85.9	4.8	143.0	96.0	83.8	3.8
C11_23	586.0	46.3	12.5	0.0482	0.0017	0.0888	0.0043	0.0132	0.0006	0.23	84.4	3.7	86.3	4.0	109.1	63.7	84.4	3.7
C11_39	1900.0	102.4	17.4	0.0470	0.0029	0.0836	0.0058	0.0132	0.0006	0.16	84.5	3.9	81.0	5.5	49.2	137.2	84.6	3.9
C11_28	211.7	41.8	5.2	0.0479	0.0012	0.0883	0.0038	0.0133	0.0006	0.39	85.3	3.7	85.9	3.6	94.8	35.1	85.3	3.7
C11_13	382.0	69.4	6.1	0.0475	0.0012	0.0871	0.0038	0.0133	0.0006	0.51	85.4	3.8	84.7	3.6	73.4	37.6	85.5	3.8
C11_30	1683.0	94.3	18.0	0.0486	0.0020	0.0881	0.0048	0.0134	0.0006	0.28	85.6	3.9	85.8	4.5	128.6	87.1	85.5	4.0
C11_31	1758.0	169.5	10.8	0.0476	0.0012	0.0884	0.0038	0.0135	0.0006	0.35	86.7	3.8	85.9	3.5	78.4	36.9	86.7	3.8
C11_29	1070.0	84.8	12.7	0.0481	0.0013	0.0893	0.0039	0.0136	0.0006	0.34	87.0	3.8	86.9	3.6	106.2	44.7	87.0	3.8
C11_24	986.0	97.7	9.9	0.0475	0.0013	0.0897	0.0040	0.0137	0.0006	0.35	87.4	3.9	87.3	3.7	73.4	47.1	87.4	3.9
C11_21	170.9	64.3	2.7	0.0547	0.0018	0.3002	0.0150	0.0402	0.0018	0.24	254.1	11.0	266.5	12.0	400.0	61.4	253.1	11.2
C11_3	56.1	18.0	3.2	0.1194	0.0028	4.5530	0.1900	0.2794	0.0130	0.63	1587.0	63.0	1740.0	35.0	1947.3	22.5	1550.4	69.9

Average weighted $^{206}Pb/^{238}U$ age of 80.4 ± 1.2 Ma (±2σ), $n = 41/48$, MSWD = 4.7, probability 1.5%

All measurement errors are given at the ±2σ level and include only errors of measurements. Decay constants and U isotope ratios: $^{238}U = 9.8485 \times 10^{-10}$, $^{235}U = 1.58125 \times 10^{-10}$, $^{238}U/^{235}U = 137.88$. In the penultimate column of the table, age is the ^{207}Pb-corrected $^{206}Pb/^{238}U$ age; (x) omitted discordant ages.
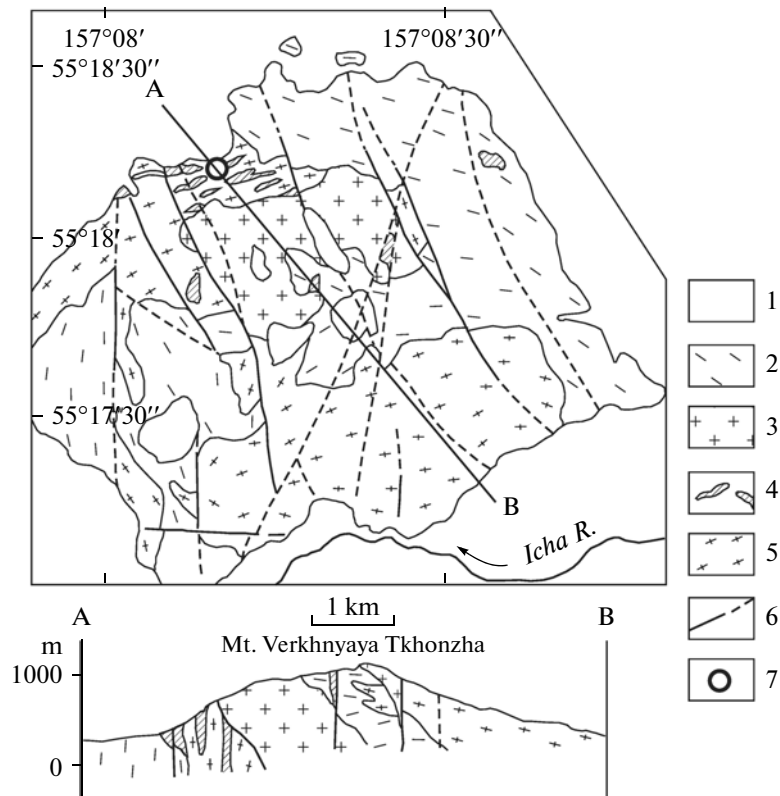
4   **Fig. 3.** Geological map of the Mount Verkhnyaya Tkhonzha massif (Shapovalenko, 1994; modified).
(1) Unconsolidated Quaternary sediments; (2) biotite−feldspar−quartz crystalline schists with garnet, staurolite, and graphite of the Kamchatka or Kolpakova groups; (3) equigranular granitoids; (4) small intrusions of the Dukuk Complex; (5) gneissic granites of the Krutogorova Complex; (6) fractures; (7) Shanuch deposit.

togorova Complex in the upper reaches of the Krutogorova River are dated back to 78.5 ± 1.2 Ma (Hourigan et al., 2009).

The samples of gneiss-like (Samples M-438/1 and M-439/1) and equigranular (Sample M-427/1) granitoids taken in the southern part of the Malka Uplift (Pravaya Kolpakova and Poperechnaya river basins) yielded ages of 83.1 ± 2.0, 76.2 ± 1.5, and 81.0 ± 1.8 Ma, respectively (Fig. 1, Table 1) (Luchitskaya and Soloviev, 2010).

In the Shanuch copper−nickel deposit area in the northern part of the Malka Uplift, gneissic granites are developed in the Mount Verkhnyaya Tkhonzha vicinity (Fig. 3) and south of the latter on the left side of the Icha River (Selyangin, 2006). The gneissic granites in the northern part of the Malka Uplift intrude the overlying sequence of crystalline schists, which may be attributed to both the Kamchatka and Kolpakova groups, and their position requires specification. Along with schists, these gneissic granitoids represent host rocks for early Eocene intrusions of the ore-bearing ultramafic−mafic Dukuk Complex (Konnikov et al., 2006; Selyangin, 2006) and equigranular granites.

Inasmuch as gneissic granites and crystalline schists are subjected to intense plicative−disjunctive dislocations and are poorly exposed, their structural relationships are best observable in the Mount Verlkhnyaya Tkhonzha area (Shapovalenko, 1994) (Fig. 3). 4 Orientation of gneissic patterns in granites and schistosity of metaterrigenous rocks demonstrate harmonic consistence indicating their joint dislocation during metamorphic transformation. The configuration of outcrops, vertical section, and drilling data allow an assumption that conformable or semiconformable gneissic granite intrusions were initially characterized by plate shapes being up to 1 km thick. One of the prospecting boreholes drilled in the Shanuch deposit penetrated at a depth of approximately 200 m their contact with the schist sequence. The contact is quenched, which is evident from the near-contact crystallization of granite in unusual rims of sillimanite and quartz−feldspar−biotite schist.

Thus, the Late Cretaceous granitoids are widespread in southern Sredinnyi Range of Kamchatka and imply that Campanian magmatism was a significant event in development of the peninsula.
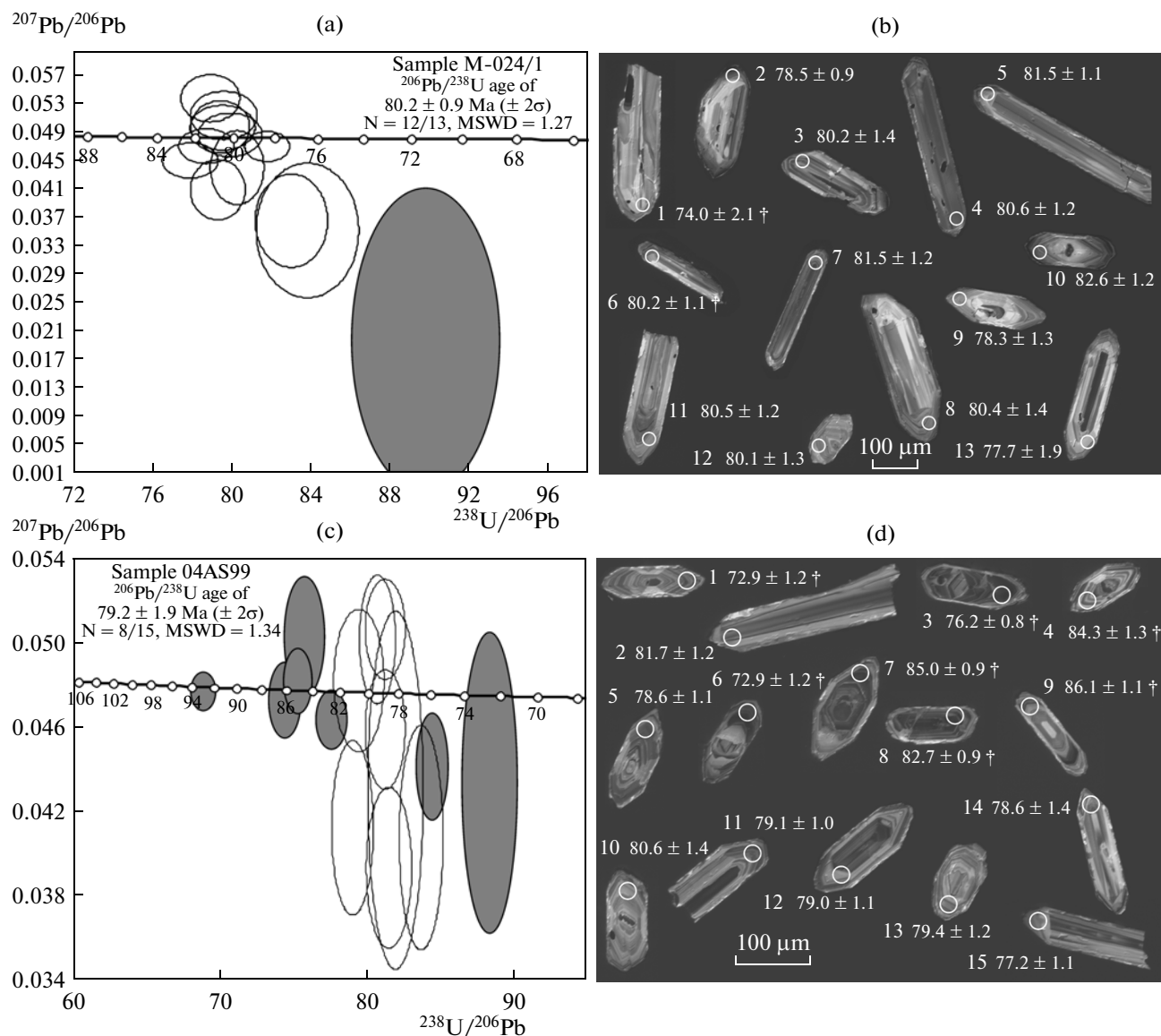
Fig. 4. Tera−Wasserburg diagrams (a, c) and cathode luminescence images of zircon grains (b, d) from Samples M-024/1 (a, b) and 04AS99 (c, d).

In diagrams, the horizontal line designates concordia, ellipses correspond to errors in measurements of ratios for each grain (±2σ), and gray color shows ellipses for discordant determinations omitted from calculations of average weighted ages. In cathode luminescence images, white circles show the points of SHRIMP analyses, and their numbers correspond to numbers of analyses in Table 2 (Sample M-024/1) and Table 3 (Sample 04AS99); age (Ma) is shown with the error of ±2σ; (†) omitted discordant ages.

ANALYTICAL METHODS

Approximately 50 zircon grains for U−Pb dating were extracted from every sample. Zircons from samples and zircons from the R33 standard were placed into epoxy resin and polished. The zircon grains were tested for the presence/absence of fissures and inclusions in reflected and transmitted light at magnification ×20. For the study of zoning and internal structure of polished zircons, a cathode luminescence detector installed on a JEOL JSM 5600 scanning electron microscope was used (Figs. 4−6).

The isotopic measurements were conducted at the SHRIMP-RG (Sensitive High Resolution Ion Microprobe—Reverse Geometry) at the Stanford−USGS Microanalytical Center (http://shrimprg.stanford. edu/) in line with the standard technique (Muir et al., 1996; Ireland and Gibson, 1998). In this technique, a beam of negative oxygen molecules ~30 μm in diameter is used for ionization of the analyzed crystal. The individual $^{206}Pb/^{238}U$ measurements are characterized by an analytical accuracy of 2%, which is higher for older grains, where the $^{207}Pb/^{206}Pb$ value is measured with a lower error. The lower ^{207}Pb content in young
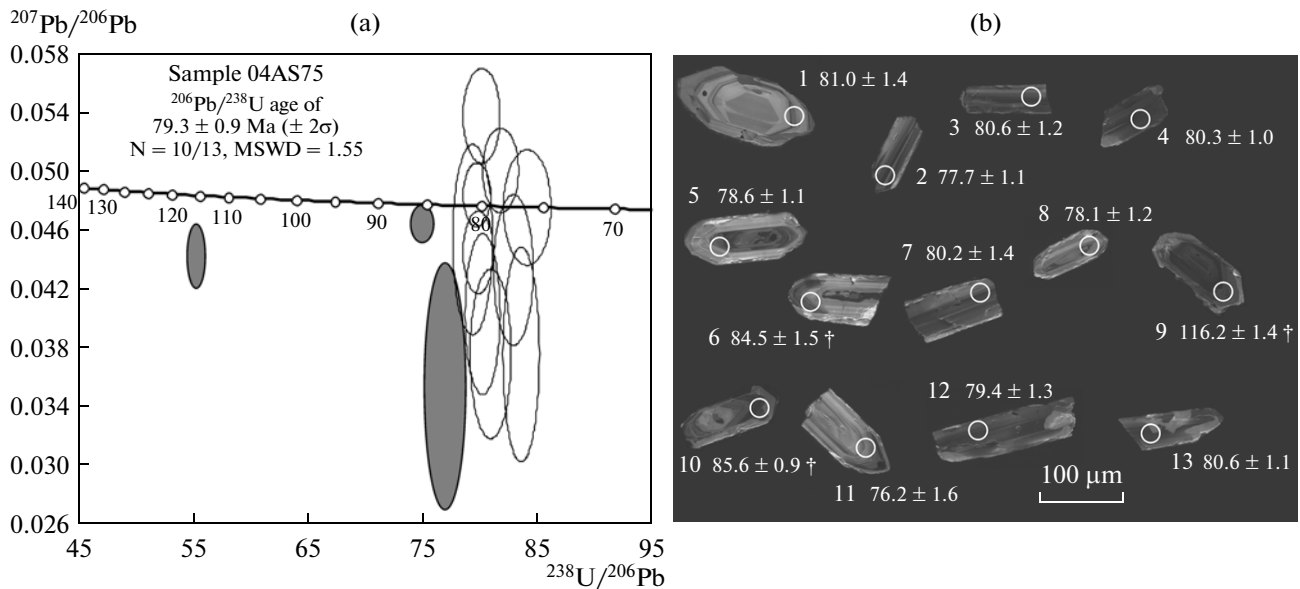
Fig. 5. Tera−Wasserburg diagrams (a, c) and cathode luminescence images of zircon grains (b) from Sample 04AS75.

In diagrams, the horizontal line designates concordia, ellipses correspond to errors in measurements of ratios for each grain (±2σ), and gray color shows ellipses for discordant determinations omitted from calculations of average weighted ages. In cathode luminescence images, white circles show the points of SHRIMP analyses, and their numbers correspond to numbers of analyses in Table 2 (Sample M-024/1) and Table 3 (Sample 04AS99); age (Ma) is shown with the error of ±2σ; (†) omitted discordant ages.
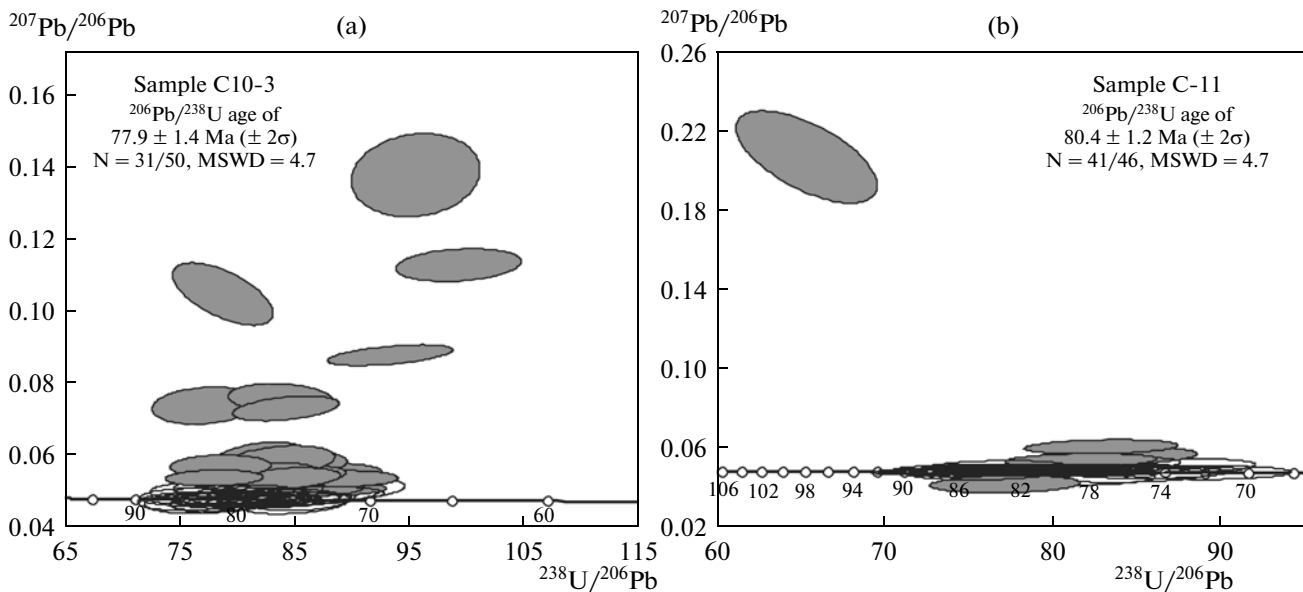
Fig. 6. Diagrams with concordia for Samples C10-3 (a) and C11 (b).

In the diagrams, ellipses correspond to errors in measurements of ratios for each grain ±2σ), and gray color shows ellipses for discordant determinations omitted from calculations of average weighted ages.

grains determines the lower accuracy of $^{207}Pb/^{206}Pb$ value measurements; therefore, the ^{207}Pb-corrected $^{206}Pb/^{238}U$ ages are accepted for grains younger than 1 Ga (Tables 2−4). The ^{207}Pb correction is based on the assumption that measured isotopic ratios reflect simple mixtures of common and radiogenic lead dur-

ing crystallization, while the measured $^{207}Pb/^{206}Pb$ value is used for the control of common lead.

The U−Pb dating of zircons by the laser ablation method (LA-SHRIMP) was performed in a laboratory of the University of California at Santa Cruz. This laboratory is equipped with an ICP-MS Element XR

spectrometer and Photon Machines Analyte.H laser ablation analyzer with the excimer laser (wavelength 193 nm) and Helex-2 camera. The evaporated substance passes through the inner Teflon tube 4 mm in diameter. The pulse energy of the ATLEX laser is 4.5 mJ. The control of energy density is provided by a calibrated attenuator. In the course of preparation of the laboratory cartridge, zircons were arranged in rows on two-sided adhesive tape using a tape matrix. Zircons of the SL2 (563 Ma; Gehrels et al., 2008) and Plešovice (337 Ma; Slama et al., 2008) standards were placed in the central part of the cartridge. Subsequently, grains were placed into the ring mold and covered with Struers Epofix epoxy resin. The hardened cartridge was cut on a turning lathe to the required size. The surface of the cartridge with zircon grains was polished first by abrasive paper with grains 1500 μm in size and then by Struers polishing pastes with grains of 9 and 3 μm on a LaboPol polishing machine.

Four measurements of the primary SL2 standard (Gehrels et al., 2008) and four measurements of the secondary Plešovice standard (Slama et al., 2008) were performed at the beginning and end of each session. The primary and secondary standards were measured after every fifth and tenth grain with unknown ages, respectively. The measurement data were processed using the Iolite for Igor Pro program (Paton et al., 2010).

The contents of major elements in rocks were determined in the Laboratory of Chemical–Analytical Investigations of GIN RAN headed by S.M. Lyapunov by the method of weight silicate analysis. The concentrations of trace elements were measured at the Institute of Mineralogy, Geochemistry, and Crystallochemistry of Rare Elements (IMGRE) by the ICP-MS method (analyst D.Z. Zhuravlev). The quality control of the ICP-MS analysis, which was realized using parallel analyses of the standard rock (BCR-2), demonstrated good accuracy and reproducibility. The detection limit for most elements with the mass exceeding 80 a.u. was approximately 0.001–0.005 ppm; for light elements, it worsened to 0.003–0.005 ppm (for beryllium). The contamination level for all the analyzed elements was negligible. All the acids used for decomposition and dilution of samples were twice recycled in quartz and Teflon devices; only deionized water was used. The samples diluted 1000 times relative to seminormal nitric acid were analyzed on a ELAN 6100 DRC mass spectrometer in the standard measurement mode (PerkinElmer, ELAN 6100, Software Kit, 2000). The measuring channels were calibrated using synthetic standards prepared from solutions of individual elements provided by PerkinElmer.

The concentrations and isotopic compositions of Sm and Nd were determined by the method of isotopic dilution at the Geological Institute (Kola Scientific Center, Russian Academy of Sciences, Apatity). Prior to decomposition of samples, a mixed $^{149}Sm/^{150}Nd$

tracer was added to the weighed portion being analyzed. The samples were decomposed in a HF + HNO_3 (or + $HClO_4$) mixture in Teflon weighing bottles at the temperature of 100°C in a thermostat up to complete dissolution. The further extraction of Sm and Nd was performed in line with the standard technique of two-step ion exchange and extraction–chromatographic separation using Dowex 50 × 8 ion exchange resin in chromatographic columns with 2.3 N and 4.5 HCl as an eluent. The selected Sm and Nd fractions were transferred into the nitrate form to receive preparations ready for the mass spectrometric analysis. All the measurements of the Nd isotope composition and concentrations of Sm and Nd by the method of isotope dilution were conducted on a seven-channel solid-phase Finnigan-MAT 262 (PRQ) mass spectrometer in a static double-band mode in collectors using Ta + Re filaments. The Re filaments were used as ionizers, while a sample was placed on the Ta filament, preliminarily covering the latter with diluted H_3PO_4. The error in the measurement reproducibility of 11 analyses of the Nd La Jolla = 0.511833 ± 6 standard (2σ, $n = 11$) never exceeded 0.0024% (2σ). Similar accuracy was characteristic of measurements of 44 parallel analyses of the Japan $JNd_i1 = 0.512072 ± 2$ standard (2σ, $n = 11$). The error in measurements of $^{147}Sm/^{144}Nd$ values in statistical calculations of Sm and Nd concentrations in the BCR-1 standard is 0.2% (2σ): average for seven measurements. The blank laboratory contamination was 0.3 and 0.06 ng for Nd and Sm, respectively. The measured Nd isotope ratios are normalized relative to $^{148}Nd/^{144}Nd = 0.241570$ and then recalculated for the $^{143}Nd/^{144}Nd$ value in the La Jolla = 0.511860 standard.

ZIRCON U–PB GEOCHRONOLOGY

Zircons from Samples M-024/1, 04AS99, and 04AS75 were analyzed by the SHRIMP-RG U–Pb method at the Stanford–USGS Microanalytical Center (http://shrimprg.stanford.edu/). Zircons from Samples C10-3 and C-11 are dated by the LA-ICP-MS U–Pb method in the laboratory of the University of California at Santa Cruz.

The gneissic biotite granites (Sample M-024/1, Fig. 1) taken in the middle reaches of the Pravaya Kolpakova River contain zoned zircon grains dated at 80.2 ± 0.9 Ma (Table 2, Figs 4a, 4b). Zircons from the sample of milonitized bimicaceous granite (04AS99) taken on the western slope of the Sredinnyi Range near the fault that separates metamorphosed and nonmetamorphosed rocks yielded an age of 79.2 ± 1.9 Ma (Table 3, Figs. 4c, 4d). The concordant age of zircons from orthogneisses (Sample 04AS75) cropping out on the right side of the Poperechnaya River is determined to be 79.3 ± 0.9 Ma (Table 4, Figs. 5a, 5b).

Sample C10-3 was taken from the drill core 50 m below the contact between granitoids and basite intrusion of the Shanuch deposit (Figs. 1, 3) (Selyangin,
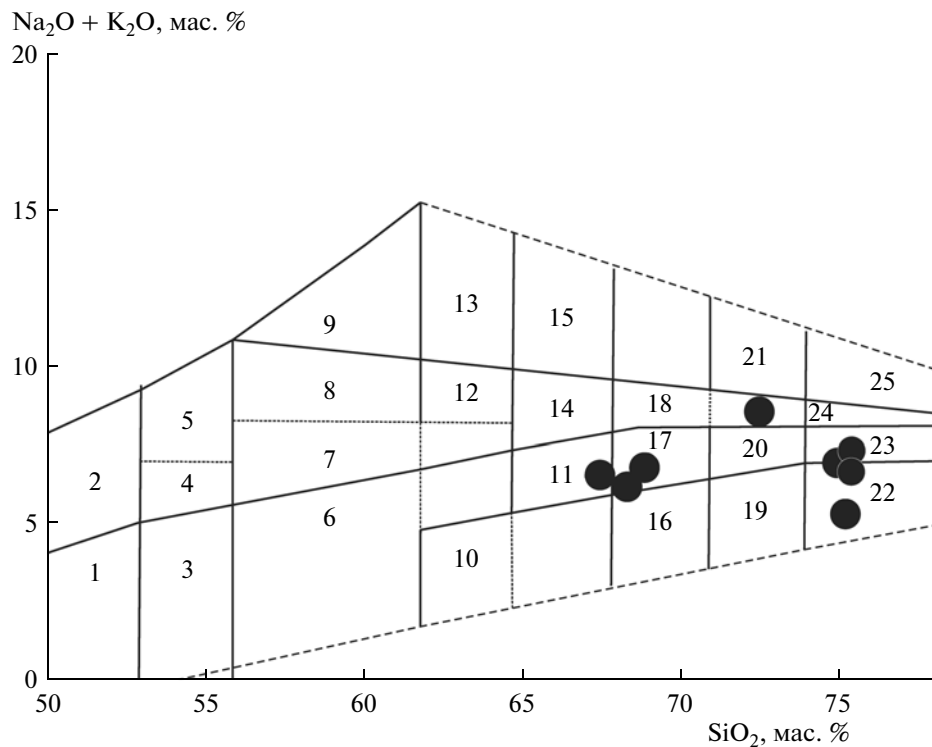
Fig. 7. Diagram (Na$_2$O+K$_2$O)−SiO$_2$ (*Petrografiya...*, 2001) for Campanian granitoids from the Malka Uplift of the Sredinnyi Range.
Fields in the diagram: (1) gabbronorites, (2) monzogabbro, (3) diorites, (4) monzodiorites, (5) monzonites, (6) quartz diorites, (7) quartz monzodiorites, (8) syenites, (9) alkaline syenites, (10) tonalities, (11) granodiorites, (12) quartz syenites, (13) alkaline quartz syenites, (14) granosyenites, (15) alkaline granosyenites, (16) trondhjemites, (17) adamellites, (18) subalkaline granites, (19) plagiogranites, (20) granites, (21) alkaline granites, (22) plagioclase leucogranites; (23) leucogranites, (24) alaskites, (25) alkaline alaskites.

2006). Sample C-11 characterizes rock drilled 10 cm above the "hot" contact with massive ores of the Sha-nuch deposit (Figs. 1, 3). Zircons from gneissic granitoids (Sample C10-3) are dated by the LA-ICP-MS U−Pb method at 77.9 ± 1.4 Ma (Fig. 6a) and their counterparts from Sample C-11 yielded an age of 80.4 ± 1.2 Ma (Fig. 6b). Some age scatter (MSWD = 4.7) is explained by the natural heterogeneity of granitoids under consideration. No correlation is observed between concentrations of parental nuclides and age. The losses of radiogenic lead are usually characteristic of crystal segments with high U or Th concentrations, since radiogenic distortions in the crystalline lattice stimulate lead losses. No losses of radiogenic lead due to diffusion are most likely observable in the situation under consideration.

Thus, taking into consideration published and original data (Table 1), the Campanian Stage in the granite formation may confidently be defined in Kamchatka.

PETROGRAPHIC COMPOSITION AND PETROGEOCHEMICAL PROPERTIES

As was mentioned, most Campanian granitoids are characterized by a gneissic structure, which is reflected in the oriented arrangement of micaceous minerals (mainly, biotite) with relics of the primary magmatic texture. Equigranular rocks are less common.

Granitoids exhibit a hypidiomorphic texture and are represented by biotite and bimicaceous two-feldspar−quartz rocks with scattered almandine garnet or without it; accessory minerals include apatite, zircon, sphene, and orthite. Some granitoid varieties are characterized by a quartz−blastoporphyric texture reflected in the presence (35−40%) of large (up to 2.0−2.5 cm long) fusiform parallel aggregates of polygranular quartz and phenocrysts of oligoclase and orthoclase (1.2−1.5 mm across) in the quartz−feldspar fine-grained (0.2−0.5 mm) microgranoblastic groundmass with lepidoblastic bands and small mica lenses.

By proportions of silica and total alkalis, the granitoids subjected to the analysis belong to rocks of the normal series (single sample characterizes subalkaline variety) and correspond to granodiorites, adamellites, leucogranites, and subalkaline granites (*Petrografiya...*, 2001) (Fig. 7, Table 6). By the degree of Al saturation relative to the sum of Ca, K, and Na, granodiorites and adamellites are moderately aluminous rocks (alumina index ASI = 0.99−1.08); leucogranites represent a high-alumina variety (ASI = 1.16−1.20).

Table 6. Petrogenic components (wt %) and trace elements (ppm) in Campanian granitoids of the Malka Uplift in the Sredinnyi Range of Kamchatka

| Sample	M-438/1	M-424/1	M-438/4	M-427/1	M-439/1	S-11	S10-3	M-437/2
SiO_2	66.23	66.98	67.96	71.20	73.76	74.1	74.2	74.71
TiO_2	0.34	0.73	0.50	0.21	0.10	0.18	0.15	0.19
Al_2O_3	16.49	14.54	15.90	14.90	14.54	14.2	14.3	13.91
Fe_2O_3	0.73	2.00	1.54	0.70	1.52	1.07	1.05	0.42
FeO	2.92	3.45	1.73	0.86	0.66	0.97	0.61	1.64
MnO	0.06	0.07	0.07	0.04	0.04	0.037	0.039	0.04
MgO	1.62	1.23	1.67	0.65	0.44	0.48	0.37	0.78
CaO	3.51	3.28	2.96	1.54	1.00	1.0	0.86	2.76
Na_2O	4.43	3.81	3.90	4.49	4.33	4.4	4.0	4.32
K_2O	2.00	2.24	2.80	3.92	2.50	2.2	3.2	0.95
P_2O_5	0.21	0.22	0.12	0.13	0.04	0.085	0.080	0.04
L.o.i.	1.00	0.80	0.76	0.75	0.90	1.23	1.3	0.22
Sum	99.54	99.35	99.91	99.39	99.83	99.88	100.05	99.98
Be	4.0	2.2	–	7.9	1.1	2.6	2.6	1.5
V	45.0	66.9	–	23.7	7.2	9.3	7.2	20.2
Cr	26.6	25.1	–	22.3	28.7	11.6	18.5	24.0
Co	9.6	10.5	–	2.2	1.7	2.1	1.3	3.7
Ni	16.9	15.6	–	19.0	45.1	48.0	13.3	26.5
Cu	13.7	14.2	–	2.8	3.0	681	13.8	3.0
Zn	62.7	62.5	–	51.8	41.1	21	25.7	34.6
Ga	21.4	20.9	–	22.0	21.1	14.7	16.9	15.1
Rb	87	91	–	168	60	69	131	47
Sr	251	192	–	257	151	74	54	294
Y	6	42	–	9	27	20	20	5
Zr	195	396	–	75	74	60	55	30
Nb	8	10	–	6	18	5.6	9.7	4
Mo	0.8	0.8	–	0.7	0.7	1.2	1.2	0.8
Cs	4.2	4.0	–	9.2	1.3	1.9	7.4	3.3
Ba	314	632	–	446	652	436	331	185
Hf	4.8	10.1	–	2.30	2.8	2.5	2.4	1.0
Ta	0.8	0.7	–	1.11	0.3	0.83	1.06	0.4
Th	10.4	9.9	–	5.17	5.6	6.1	6.4	5.6
U	1.7	2.3	–	3.33	1.1	3.5	5.0	0.8
La	42.19	29.80	–	17.41	16.72	11.4	10.9	14.02
Ce	83.41	68.64	–	32.67	39.28	28.0	27.1	29.86
Pr	8.97	8.28	–	4.06	4.68	3.4	3.3	3.32
Nd	31.75	32.98	–	14.70	17.99	13.6	13.3	12.05
Sm	4.39	7.53	–	3.20	4.35	3.7	3.6	2.26
Eu	1.03	1.12	–	0.64	0.44	0.28	0.27	1.14
Gd	2.63	7.30	–	2.58	4.47	3.9	3.7	1.75
Tb	0.25	1.14	–	0.35	0.75	0.67	0.66	0.21
Dy	1.00	6.67	–	1.67	4.38	4.4	4.2	0.94
Ho	0.16	1.37	–	0.28	0.89	0.87	0.82	0.15
Er	0.44	3.73	–	0.64	2.34	2.6	2.5	0.38
Tm	0.07	0.56	–	0.09	0.32	0.39	0.38	0.05
Yb	0.44	3.57	–	0.52	1.90	2.6	2.6	0.28
Lu	0.07	0.53	–	0.07	0.27	0.38	0.37	0.04
La_N/Yb_N	63.56	5.59	–	22.47	5.88	2.90	2.81	33.07
Eu_N/Eu^*	0.93	0.47	–	0.69	0.31	0.23	0.23	1.77
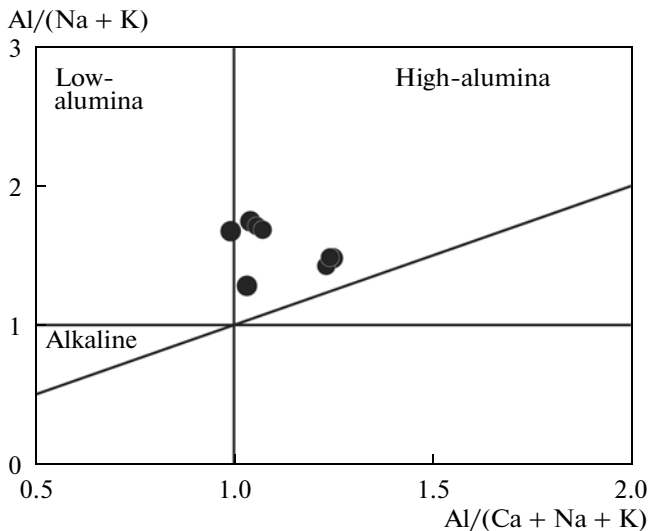
Fig. 8. Diagram Al/(Na + K)−Al/(Ca + Na + K) for Campanian granitoids from the Malka Uplift of the Sredinnyi Range.
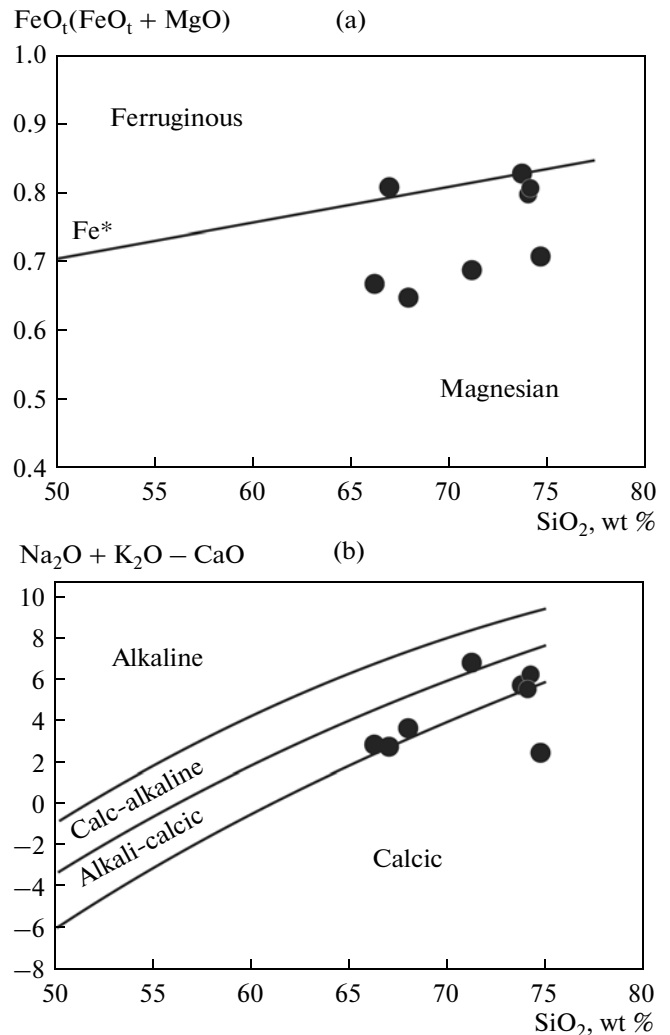

Fig. 9. Diagrams $(FeO_t/FeO_t + MgO)$−SiO_2 (a) and $(Na_2O + K_2O − CaO)$−SiO_2 (b) for Campanian granitoids from the Malka Uplift of the Sredinnyi Range.

According to the classification in (Frost et al., 2001), the granitoids under consideration belong to magneisan rocks (Fe* = $FeO_t/(FeO_t + MgO)$ = 0.65−0.81) (Fig. 9a); by the ratio of the modified Peacock index (MALI = $Na_2O + K_2O − CaO$ = 2.8−6.3) and SiO_2, they are mostly alkali-calcic. A single data point of every sample falls into the field of calc-alkaline (MALI = 6.9) and calcic (MALI = 2.5) rocks (Fig. 9b).

In the classification diagram (Whalen et al., 1987), the data points of granitoids are localized in the field of S- and I-type granites (Fig. 10a); in the Pearce diagram (Pearce et al., 1984), they fall into the field of granites of volcanic arcs being located near the boundary with a field of syncollisional granites (Fig. 10b).

Two types of chondrite-normalized spectra of the REE distribution are established for granitoids.

The first type is characterized by a fractionated REE distribution (La_N/Yb_N = 22.47−63.56) and both positive (Eu/Eu* = 1.77) and low negative (Eu/Eu* = 0.69−0.93) anomalies (Fig. 11a).

Granitoids of the second type exhibit a moderately fractionated REE distribution and a distinct negative Eu anomaly (La_N/Yb_N = 2.81−5.88, Eu/Eu* = 0.23−0.47) (Fig. 11b). The distribution spectra of granitoids are similar to the spectrum characteristic of host metaterrigenous rocks of the Kolpakova Group, differing from the latter in a deeper negative Eu anomaly (Fig. 11b), and the spectrum characteristic of the Manaslu leucogranites of the Himalayas (Crawford and Windley, 1990), differing from it in higher total REE contents.

The spider diagrams of chondrite-normalized trace elements compiled for granitoids with different REE distribution spectra demonstrate the trend in common: they are enriched in lithophile elements (LILE) relative to high field strength elements (HSFE) and characterized by Rb, Th, La, and Ce maxima, Ba, Nb, Sr, P, and Ti minima, and different concentrations of heavy REE elements and Y (Figs. 12a, 12b).

Four samples of bimicaceous and biotite granites and four samples of metamorphic rocks from the Kamchatka Group represented by biotite and bimicaceous schists with garnet were subjected to the Sm−Nd and Rb−Sr isotope analysis (Table 7). Granites differ insignificantly from each other in the Nd isotope composition and exhibit low positive (from 0.85 to 1.59) and negative (−0.36) $\varepsilon_{Nd}(T)$ values. The $^{87}Sr/^{86}Sr$ isotope ratios determined in two granite samples are 0.705465 and 0.706303. The $T_{Nd}(DM)$ ages obtained for granites vary from 590 to 993 Ma. The rocks of the Kamchatka Group are largely characterized by lower negative $\varepsilon_{Nd}(T)$ values ranging from −1.63 to −3.2 and higher
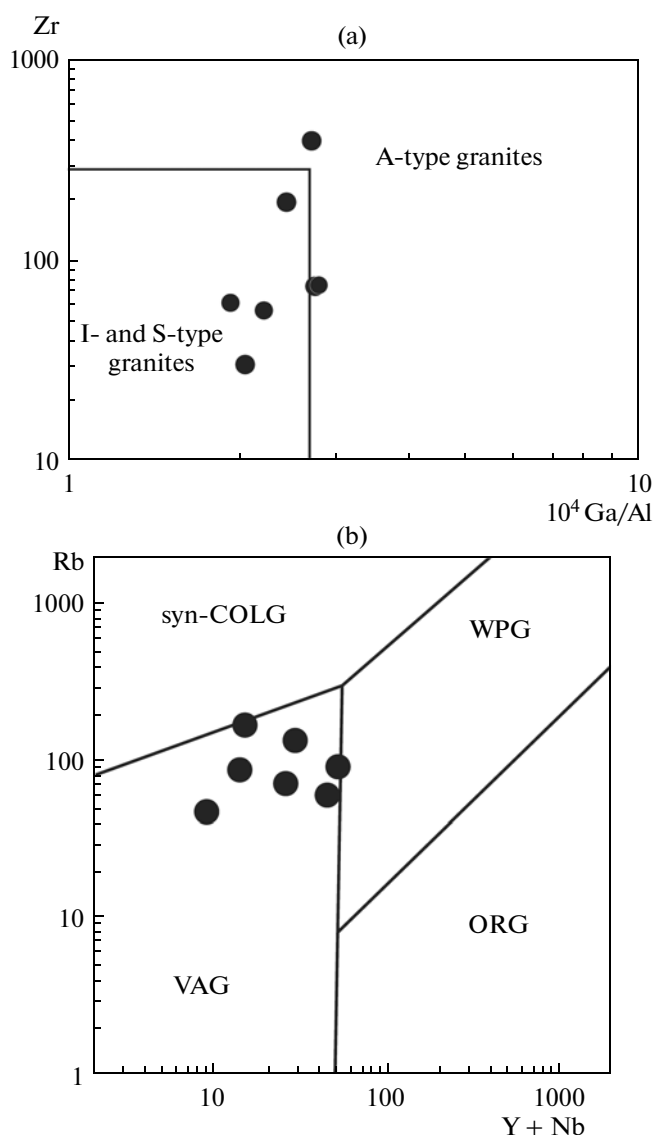
Fig. 10. Diagrams Zr–10^4Ga/Al (Whalen et al., 1987) (a) and Rb–(Y + Nb) (Pearce et al., 1984) (b) for Campanian granitoids from the Malka Uplift of the Sredinnyi Range. (b) Types of granites: (syn-COLG) syncollisional, (VAG) volcanic arcs, (WPG) intraplate, (ORG) oceanic ridges.

^{87}Sr/^{86}Sr isotope ratios (from 0.706226 to 0.7079470); their T_{Nd}(DM) ages vary from 1033 to 1660 Ma.

DISCUSSION

By their petrographic composition and petrochemical properties, the Campanian granitoids represent rocks intermediate between I- and S-type granites (Chappell and White, 1992). The features in common with I-type granites are the occurrence of granodiorites and adamellites, where dark-colored mineral is represented by biotite; values of Fe* <0.8, which allow these granitoids to be attributed to magnesian rocks

(Fig. 9a); elevated Sr, Ba, and V concentrations; lowered Rb contents (Table 6); Zr and Ga/Al ratios (Fig. 10a); similarity to granites of volcanic arcs by the Rb and Y + Nb ratios (Fig. 10b); Nd isotope composition; and low ^{87}Sr/^{86}Sr values (<0.708). At the same time, the presence of leucogranites with high SiO$_2$ contents, occurrence of muscovite and garnet, and high alumina index emphasize the similarity of Campanian granitoids to S-type granites.

It is shown (Chappell et al., 2012) that half of all the low-temperature I-type granites of eastern Australia contain high-alumina varieties along with more mafic low-alumina granitoids. The authors of the last work believe that, according to experimental investigations, melts generated during partial melting of basaltic or andesitic material in crustal environments are dominated by high-alumina varieties. During dehydration melting of source material of I-type granites under pressures below the stability limit of garnet, biotite and amphibole are melted in the incongruent mode to form pyroxene. The Al excess becomes transferred to the melt, which acquires high-alumina properties. In the opinion of Chappel et al. (2012), transformation of high-alumina granitoids into low-alumina varieties may occur in substantially closed isotopic systems either under growing melting temperatures, or dissolution of calcium and other components of pyroxene, or capture of restite minerals (pyroxenes and plagioclase) by the melt, which results in a lowered alumina index of the melt. Thus, according to the classification in (Chappell et al., 2012), the Campanian granitoids should likely be attributed to high-alumina I-type granites.

The REE distribution spectra in adamellite and leucogranites with a low La$_N$/Yb$_N$ value and distinct negative Eu anomaly (Samples C-11, C10-3, M-424/1, M-439/1) are similar to their counterparts for granites, which are thought to be produced by partial melting of the metasedimentary protolith, such as Miocene syncollisional Manaslu leucogranites of the Himalayas (Crawford and Windley, 1990). The similarity between the REE distribution spectra in granitoids and host metaterrigenous rocks of the Kolpakova Group and overlying matorrigenous rocks of the Kamchatka Group confirms this assumption (Fig. 11b). According to (Rikhter, 1995), primary rocks of the Kolpakova Group were greywacke in composition, while rocks of the Kamchatka Group were represented by clays with rare intercalations of polymictic to arkosic sandstones (Tararin, 1988, 2008).

The fractionated REE spectra of granodiorites and adamellites depleted in heavy lanthanides, with high La$_N$/Yb$_N$ ratio, and without or with positive Eu anomaly (Samples M-438/1, M-427/1, M-437/2; Fig. 11a) allow an assumption that granitoids were melted in equilibrium with the restite containing garnet and (or) hornblende and at a deeper level as compared with that of leucogranites. Such spectra are characteristic of high-alumina tonalities, trondhjemites, and grano-
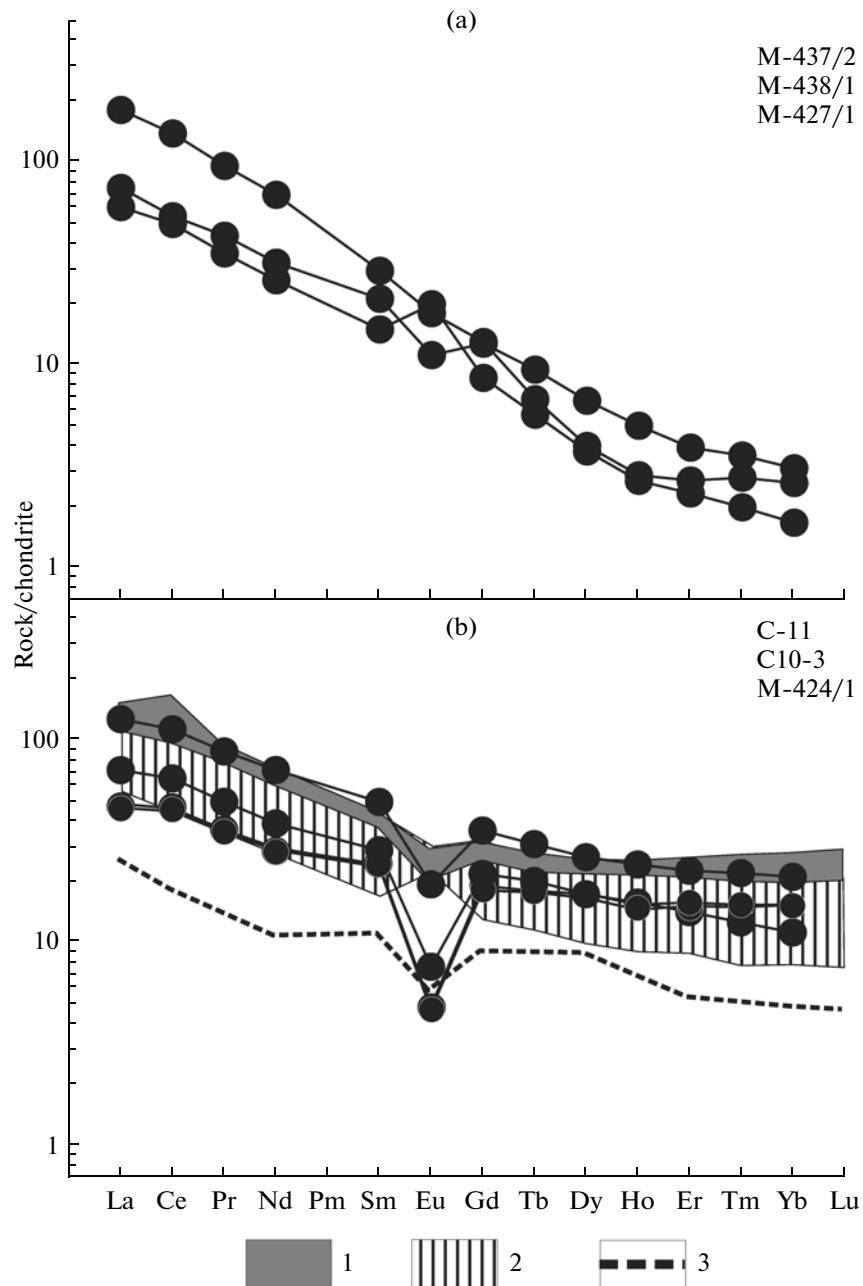
Fig. 11. Chondrite-normalized (after Sun and Donough, 1989) REE spectra of Campanian granitoids from the Malka Uplift of the Sredinnyi Range.
(a) Samples M-438/1, M-427/1, M-437/1; (b) Samples C-11, C10-3, M-424/1, M-439/1. (1, 2) Metaterrigenous rocks of the Kolpakova (1) and Kamchatka (2) groups, (3) Miocene Manaslu leucogranites, Himalayas (Crawford and Windley, 1990).

diorites obtained by experimental partial melting of metabasites (e.g., Rapp and Watson, 1995).

As was mentioned, the Kolpakova Group intruded by Campanian granitoids may represent an analog of near-continental subduction–accretionary wedges; this is evident from the occurrence of lenticular bodies of amphibolites, which originated from oceanic basalts, and metacarbonate rocks among dominant metaterrigenous sequences. Thus, the melted source of Campanian granitoids could include both sedimentary material of the accretionary wedge and fragments of basalts enclosed in the latter.

The insignificant variations of the Nd isotope composition in granitoids indicate that their crustal protolith should be close in age. The negligible (-0.36) or low positive $\varepsilon_{Nd}(T)$ values (up to 1.59)
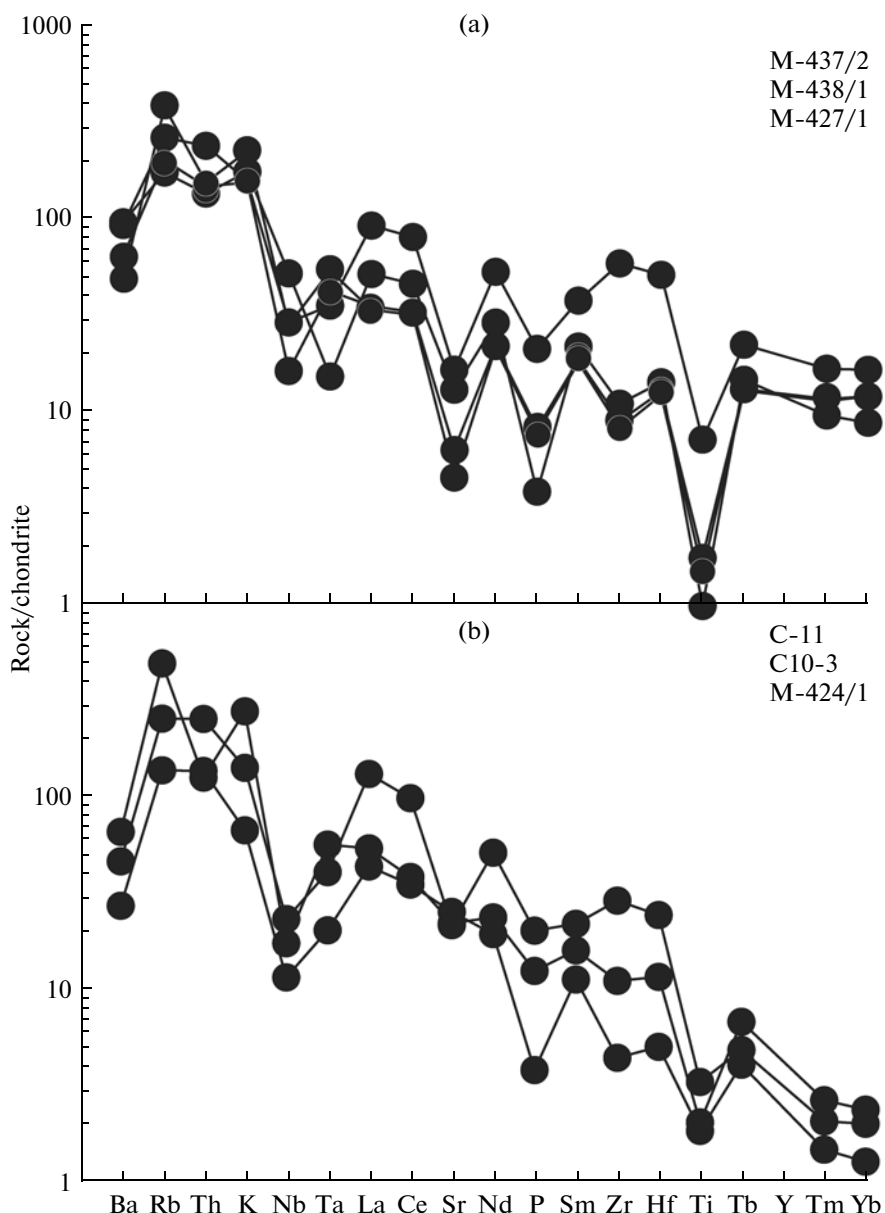
Fig. 12. Spider diagrams of chondrite-normalized (Sun and Donough, 1989) trace elements in Campanian granitoids.
(a) Samples M-438/1, M-427/1, M-437/1; (b) Samples C-11, C10-3, M-424/1, M-439/1.

combined with low $^{87}Sr/^{86}Sr$ isotope ratios (0.706303, 0.705465) as well as model ages of granitoids (590−993 Ma) suggest that the rocks under consideration were formed from sources with a brief crustal prehistory and that granitoid magmas avoided a contribution of ancient crustal material to their formation during melting.

CONCLUSIONS

The geochronological data indicate that Late Cretaceous granitoids (from 83.1 ± 2.0 to 76.2 ± 1.5 Ma) are widespread in the southern Sredinnyi Range of Kamchatka. This allows the Campanian stage in magmatic activity of southern Kamchaka to be defined, considering the latter as marking the onset of production of the "newly formed" continental crust. By their petrographic composition and petrogeochemical properties, the Campanian granitoids may be correlated with high-alumina I-type granites, according to the classification in (Chappell et al., 2012). The data on the structure and composition of host rocks allow an assumption that granitoids intruded into complexes of the accretionary wedge, while the REE distribution

Table 7. Sm−Nd isotope data on Campanian granitoids from the southern Sredinnyi Range of Kamchatka

Sample	Description	Sm, ppm	Nd, ppm	$^{147}Sm/^{144}Nd$	$^{143}Nd/^{144}Nd$	$\varepsilon_{Nd}(T)$	T_{Nd} (DM) @Млн лет	Rb, ppm	Sr, ppm	$^{87}Rb/^{86}Sr$	$^{87}Sr/^{86}Sr$
M-427/1	Bi−Mu granite	4.966	28.05	0.10699	0.512589	−0.36	804	152.2	235.7	1.86843	0.706303
M-424/2	Bi gneissic granite	7.473	33.57	0.134565	0.512687	1.59	895	−	−	−	−−
M-439/1	Bi−Mu granite with Gar	4.480	19.81	0.136669	0.51265	0.85	993	−	−	−	−
M-438/1	Bi gneissic granite	4.238	31.04	0.08254	0.512644	1.28	590	83.41	229.1	1.05328	0.705465
M-445/1	Bi schist	3.070	12.37	0.15001	0.512457	−3.2	1660	144.2	281.5	1.48282	0.707947
M 439/2	Bi schist with Gar	5.948	29.57	0.12158	0.512527	−1.63	1033	53.68	353.3	0.43963	0.706226
M 422/1	Bi−Mu schist with Gar	5.934	28.89	0.12417	0.51245	−3.16	1194	77.16	258.7	0.86291	0.707372
M 415/1	Bi−Mu schist with Gar	6.591	31.21	0.12764	0.512454	−3.1	1235	84.96	286.0	0.85936	0.706764

spectra imply a contribution of both sedimentary and basaltic material to their petrogenesis.

REFERENCES

1 Bindeman, I.N., Vinogradov, V.I., Valley, J.W., et al., Archean protolith and accretion of crust in Kamchatka: SHRIMP dating of zircons from Sredinny and Ganal Massifs, *J. Geol.,* 2002, vol. 110, pp. 27−289.

Bondarenko, G.E., Ultramafic and mafic metavolcanites in the Sredinnyi Range of Kamchatka: position in the section and formation setting, *Byull. Mosk. O−va Ispyt. Prir., Otd. Geol.*, 1997, vol. 72, no. 3, pp. 32−40.

Chappell, B.W. and White, A.J.R., I− and S−type granites in the Lachlan Fold Belt, *Trans. Roy. Soc. Edinburgh: Earth Sci.*, 1992, vol. 83, pp. 1−26.

Chappell, B.W., Bryant, C.J., and Wyborn, D., Peraluminous I−type granites, *Lithos*, 2012, vol. 158, pp. 142−153.

2 Crawford, M.B. and Windley, B.F., Leucogranites of the Himalaya/Karakoram: implications for magmatic evolution within collisional belts and the study of collision-related leucogranite petrogenesis, *J. Volcanol. Geotherm. Res.*, 1990, vol. 44, pp. 1−19.

Frost, B.R., Barnes, C.G., Collins, W.J., et al., A geochemical classification for granitic rocks, *J. Petrol.*, 2001, vol. 42, no. 11, pp. 2033−2048.

Gehrels, G.E., Valencia, V., and Ruiz, J., Enhanced precision, accuracy, efficiency, and spatial resolution of U-Pb ages by laser ablation-multicollector-inductively coupled plasma-mass spectrometry, *Geochem. Geophys. Geosyst.*, 2008, vol. 9, Q03017. doi: 10/1029/2007GC001805

Gosudarstvennaya geologicheskaya karta Rossiiskoi Federatsii. Ob"yasnitel'naya zapiska. Masshtab 1 : 1 000 000 (tret'e pokolenie). List N-57 - Petropavlovsk-Kamchatskii (The 1 : 1 000 000 State Geological Map of the Russian Federation (the 3rd ed.). Sheet N-57—Petropavlovsk-Kamchatsky. Explanatory Note), Litvinov, A.F. and Markovskii, B.A., Eds., St. Petersburg: VSEGEI, 2006 [in Russian].

Hourigan, J.K., Brandon, M.T., Soloviev, A.V., et al., Eocene arc-continent collision and crustal consolidation in Kamchatka, Russian Far East, *Am. J. Sci.*, 2009, vol. 309, pp. 333−396.

Ireland, T.R. and Gibson, G.M., SHRIMP monazite and zircon geochronology of high-grade metamorphism in New Zealand, *J. Metam. Geol.*, 1998, vol. 16, pp. 149−167.

Karta poleznykh iskopaemykh Kamchatskoi oblasti. Masshtab 1 : 500 000 (The 1 : 500 000 Map of Mineral Resources of the Kamchatka Oblast), Litvinov, A.F., Patoka, M.G., Markovskii, B.A., Eds., St. Petersburg: VSEGEI, 1999 [in Russian].

Khanchuk, A.I., *Evolyutsiya drevnei sialicheskoi kory v ostrovoduzhnykh sistemakh vostochnoi Azii* (Evolution of Ancient Sialic Crust in the Island-Arc Systems of East Asia), Vladivostok: DVNTs AN SSSR, 1985 [in Russian].

Hourigan, J.K., Soloviev, A.V., Ledneva, G.V., et al., Timing of syenite intrusions on the eastern slope of the Sredinny Range, Kamchatka: rate of accretionary structure exhumation, *Geochem. Int.*, 2004, vol. 42, no. 2, pp. 97−105.

Kirmasov, A.B., Soloviev, A.V., and Hourigan, J.K., Collision and postcollision structural evolution of the Andrianovka Suture, Sredinny Range, Kamchatka, *Geotectonics*, 2004, vol. 38, no. 4, pp. 294–316.

3 Konnikov, E.G., Chubapov, V.M., Tpavin, V.A., et al., Formation time of the Ni-bearing norite-cortlandite association of East Asia, *Geochem. Int.*, 2006, no. 5, pp. 516–521.

Kuz'min, V.K., Shokal'skii, S.P., Rodionov, N.V., and Sergeev, S.A., New U-Pb age data on Kamchatka metabasites, in *Vulkanizm i geodinamika. Mat. IV Vseross. simp. po vulkanologii i paleovulkanologii* (Proc. IV All-Rus. Symp. on Volcanology and Paleovolcanology "Volcanism and Geodynamics"), Petropavlovsk-Kamchatsky: IViS DVO RAN, 2009, vol. 1, pp. 388–391.

Lebedev, M.M., Upper Cretaceous crystalline schists of Kamchatka, *Sov. Geol.*, 1967, no. 4, pp. 57–69.

Luchitskaya, M.V., Soloviev, A.V., and Hourigan, J.K., Two stages of granite formation in the Sredinny Range, Kamchatka: Tectonic and geodynamic setting of granitic rocks, *Geotectonics*, 2008, vol. 42, no. 4, pp. 286–304.

Luchitskaya, M.V. and Soloviev, A.V., Campanian Stage of granite formation in the south of the Sredinny Range in Kamchatka: new U–Pb SHRIMP data, *Dokl. Earth Sci.*, 2010, vol. 430, no. 3, pp. 22–27.

Luchitskaya, M.V. and Soloviev, A.V., Early Eocene magmatism in the Sredinny Ridge of Kamchatka: composition and geodynamic aspects, *Petrology*, 2012, vol. 20, no. 2, pp. 147–187.

Marchenko, A.F., Tectonic nature, age, and structural position of metamorphic complexes of Kamchatka, in *Voprosy magmatizma i tektoniki Dal'nego Vostoka* (Problems in Magmatism and Tectonics of the Far East), Vladivostok: DVNTs AN SSSR, 1975, pp. 234–246.

Muir, R.J., Ireland, T.R., Weaver, S.D., and Bradshaw, J.D., Ion microprobe dating of Paleozoic granitoids: Devonian magmatism in New Zealand and correlations with Australia and Antarctica, *Chem. Geol.*, 1996, vol. 127, nos. 1–3, pp. 191–210.

Paton, C., Woodhead, J.D., Hellstrom, J.C., et al., Improved laser ablation U–Pb zircon geochronology through robust downhole fractionation correction, *Geochem. Geophys. Geosyst.*, 2010, vol. 11, Q0AA06. doi: 10.1029/2009GC002618

Pearce, J.A., Harris, N.B.W., and Tindle, A.G., Trace element discrimination diagrams for the tectonic interpretation of granitic rocks, *J. Petrol.*, 1984, vol. 25, no. 4, pp. 956–983.

*Petrografiya i petrologiya magmaticheskikh, metamorficheskikh i metasomaticheskikh gornykh porod (*Petrography and Petrology of Magmatic, Metamorphic, and Metasomatic Rocks), Popov, V.S. and Bogatikov, O.A., Eds., Moscow: Logos, 2001 [in Russian].

Rapp, R.P. and Watson, E.B., Dehydration melting of metabasalt at 8–32 kbar: implications for continental growth and crust-mantle recycling, *J. Petrol.*, 1995, vol. 36, pp. 891–931.

Rikhter, A.V., Structure of metamorphic complex of the Central Kamchatka massif, *Geotectonics*, 1995, vol. 95, no. 1, pp. 65–72.

Selyangin, O.B., Cortlandite–amphibole pyroxenite–hornblendite series of the Ni-bearing layered Vostochno-Geofizichesky Intrusion, Shanuch Ore Field, Kamchatka, *Vestn. KRAUNTs. Nauki o Zemle*, 2006, no. 2, Iss. 8, pp. 9–29.

Selyangin, O.B., Tectonic Position of the Ni-bearing Intrusions of the Sredinnyi Massif of the Kamchatka, *Vestn. KRAUNTs. Nauki o Zemle*, 2009, vol. 13, no. 1, pp. 123–138.

Shapiro, M.N., Soloviev, A.V., and Hourigan, J.K., Lateral structural variability in zone of Eocene Island-Arc–Continent collision, *Geotectonics*, 2008, vol. 42, no. 6, pp. 469–487.

Shapovalenko, V.N., *Otchet o rezul'tatakh poiskovo-otse-* 4 *nochnykh rabot na Shanuchskom mestorozhdenii za 1991-1994 gody* (The Report on the Results of Prospect Evaluation Works at the Shanuch Ore Field during 1991—1994), Petropavlovsk-Kamchatsky: FGU "TFI po Kamchatskoi oblasti i KAO," 1994 [in Russian].

Slama, J., Kosler, J., Condon, D.J., et al., Plesovice zircon—a new natural reference material for U–Pb and Hf isotopic microanalysis, *Chem. Geol.*, 2008, vol. 249, pp. 1–35.

Soloviev, A.V., Hourigan, J.K., Brendon, M.T., et al., The Age of the Baraba Formation inferred from the U/Pb (SHRIMP) Dating (Sredinnyi Range, Kamchatka): geological consequences, *Stratigr. Geol. Correl.*, 2004, vol. 12, no. 4, pp. 418–424.

Soloviev, A.V., Palechek, T.N., Shapiro, M.N., et al., New data on the Baraba Formation age (the Sredinnyi Range of Kamchatka), *Stratigr. Geol. Correl.*, 2007, vol. 15, no. 1, pp. 112–119.

Soloviev, A.V., *Izuchenie tektonicheskikh protsessov v oblastyakh konvergentsii litosfernykh plit: metody trekovogo datirovaniya i strukturnogo analiza* (Study of Tectonic Processes in Zones of Convergent Lithospheric Plates: Methods of Fission Track Dating and Structural Analysis), Moscow: Nauka, 2008 [in Russian].

Sun, S.S. and McDonough, W.F., Chemical and isotope systematics of oceanic basalts: implications for mantle composition and processes, in *Magmatism in the Oceanic Basins*, Saunders A.D. and Norry M.J., Eds., *Geol. Soc. Spec. Publ.*, 1989, vol. 42, pp. 313–345.

Tararin, I.A., Evolution of the metamorphic processes in the Sredinnyi Kamchatka Metamorphic Zone, *Tikhookean. Geol.*, 1988, no. 1, pp. 63–70.

Tararin, I.A., Granulites of the Kolpakovskaya Series in the Sredinnyi Range, Kamchatka: A myth or reality? *Petrology*, 2008, vol. 16, no. 2, pp. 193–209.

Whalen, J.B., Currie, K.L., and Chappell, B.W., A-type granites: geochemical characteristics, discrimination, and petrogenesis, *Contrib. Mineral. Petrol.*, 1987, vol. 95, pp. 407–419.

Zhegalova, G.V., New data on tectonic structure of the Central Kamchatka (Khim–Kirganik Ore Zone), *Tr. Vsesoyuz. Zaochn. Politekhn. Inst.*, 1978, no. 117, pp. 116–118.

Zhegalova, G.V., Melange in the massifs of the gabbronorite–cortlandite complex of the Sredinnyi Range of Central Kamchatka, *Geotectonika*, 1981, no. 3, pp. 105–111.

Translated by I. Basov

SPELL: 1. Bindeman, 2. Windley, 3. Chubapov, 4. Shapovalenko